# Increased neuron density in the midbrain of foveate birds results from profound change in tissue morphogenesis

Tania Rodrigues[1], Linda Dib[2], Émilie Bréthaut[3], Michel M. Matter[4], Lidia Matter-Sadzinski[1], and Jean-Marc Matter[1]

[1] Department of Molecular Biology & Department of Biochemistry, Sciences III, University of Geneva, 30 quai Ernest-Ansermet, 1211 Geneva 4, Switzerland

[2] Swiss Institute of Bioinformatics, Le Génopode, 1015 Lausanne, Switzerland

[3] La Vaux-Lierre, 1163 Etoy, Switzerland

[4] HEPIA, HES-SO, University of Applied Sciences and Arts Western Switzerland, 1202 Geneva, Switzerland.

## Graphical Abstract

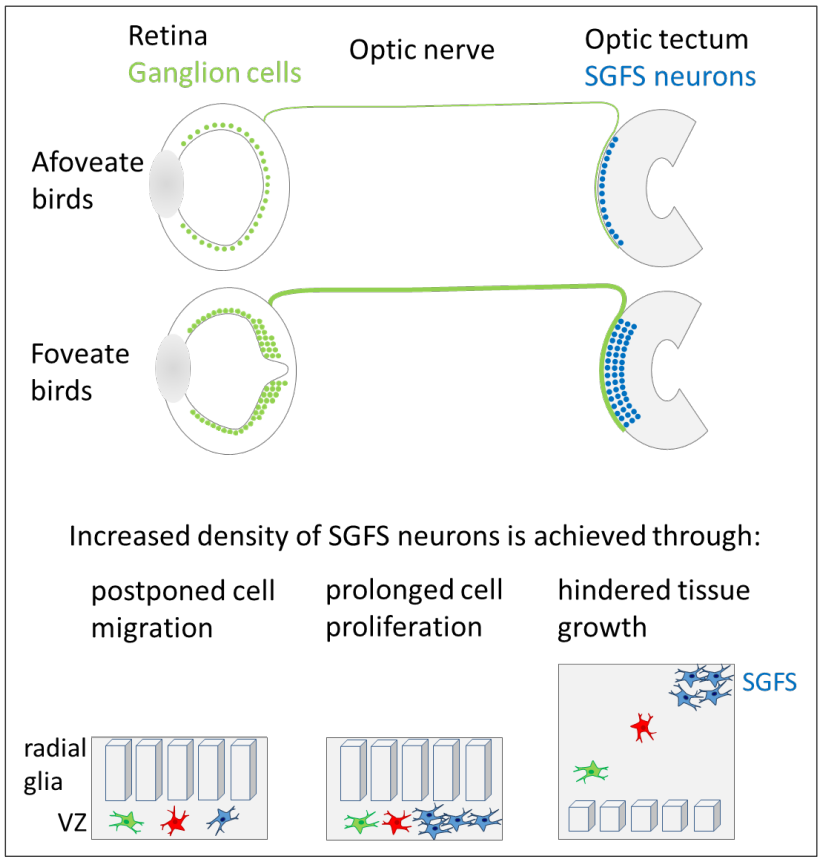


## Correspondance

Tania.Rodrigues@unige.ch (T.R.)

Jean-Marc.Matter@unige.ch (J.-M.M.)

## Highlights

- The presence of a fovea is associated with increased neuron density in the optic tectum
- Fovea number and deepness influence neuron density in the optic tectum
- Increased neuron density in the upper layers of the optic tectum requires major developmental changes
- Postponed cell migration, prolonged cell proliferation, hindered tissue growth are necessary settings for achieving high neuron density

SUMMARY

The increase of brain neuron number in relation with brain size is currently considered to be the major evolutionary path to high cognitive power in amniotes. However, how changes in neuron density did contribute to the evolution of the information-processing capacity of the brain remains unanswered. High neuron densities are seen as the main reason why the fovea located at the optical center of the retina is responsible for sharp vision in birds and primates. The emergence of foveal vision is considered as a breakthrough innovation in visual system evolution. We found that neuron densities in the largest visual center of the midbrain – i.e., the optic tectum – are two to four times higher in modern birds with one or two foveae compared to birds deprived of this specialty. Interspecies comparisons enabled us to identify elements of a hitherto unknown developmental process set up by foveate birds for increasing neuron density in the upper layers of their optic tectum. The progenitor cells that generate these neurons proliferate in a ventricular zone that can expand only radially. In this particular context, the number of cells in ontogenetic columns increases, thereby setting the conditions for higher cell densities in the upper layers once neurons did migrate.

## INTRODUCTION

High visual acuity in primates is restricted to central vision, while acuity is low in the periphery. A major reason is that the density of retinal ganglion cells (RGCs) falls precipitously away from the fixation point, i.e., the fovea. About half of the ~$1.2\times10^6$ RGCs in the human retina are located in the fovea, which represents less than 1% of the total retinal surface (Bringmann et al., 2018; Provis et al., 2013). RGCs whose bundled axons make up the optic nerve transmit visual information from the retina to the brain. While it is well known that the fovea makes primate visual perception unique among mammals, what is less well known is that this retinal specialization is of paramount importance for spatial and temporal acuities in birds of the Neoaves clade encompassing ~95% of the ~10'500 bird species (Bringmann, 2019; Jarvis et al., 2014; Prum et al., 2015). The recognition that the fovea is a region for acute vision dates back to the end of the 19th century (Ramón y Cajal, 1893; Slonaker, 1897). Despite this early interest, we know very little about neural signaling in the fovea. In birds, the optic tectum (OT) is the largest visual center and its twin lobes form the roof of the midbrain. RGC axons terminate in the superficial layers of the contralateral lobe where they establish connections with upper neurons of the stratum griseum et fibrosum superficiale (SGFS). Retinal inputs are retinotopically distributed over the tectal surface. Electrophysiological recordings have shown that the foveal projection in the lateral geniculate nucleus, the superior colliculus and the primary visual cortex (V1) of primates and on the tectal surface of birds is a region of increased areal magnification (Clarke and Whitteridge, 1976; Cowey and Rolls, 1974; Daniel and Whitteridge, 1961; Malpeli and Baker, 1975; Rolls and Cowey, 1970; Rosa et al., 1997). It is assumed that because of the high number and high density of RGCs in their fovea, primates must have more neurons in V1 than non-primate mammals to account for the differences in acuity. Quantitative evaluations of cell number and density indicate that primates increase the number of neurons by increasing their density in the V1 area (Collins et al., 2010; Rockel et al., 1980; Srinivasan et al., 2015). However, the fact that in the Grey Mouse Lemur (*Microcebus murinus*) V1 occupies more than 20% of the neocortical area, the highest described in the primates to date (Ho et al., 2021) raises the possibility that increasing the V1 area could also contribute to increase the number of neurons. Thus, it is still unclear to what extent the increase of neuron density in the visual areas of the brain contributes to the enhanced representation of the fovea. To address this question, we asked how the OT of birds did adapt to the increased number of retinal inputs. First, we measured the surface density of neurons in the SGFS of birds who have one or two foveae or who are deprived of this retinal specialty. We found that cell densities were two to four times higher in the foveate birds. Although the retinal histology of less than one hundred bird species has been reported so far, we can reasonably assume that the fovea is one trait that distinguishes Neoaves from

Galloanserae. Unlike the Galloanserae, which are precocial, the majority of modern birds are altricial, i.e., birds hatch with closed eyes and require prolonged parental care. Altriciality, by changes in the rate of development, may help to relax constraints on the duration of ontogenesis, a precondition for brain expansion and cognitive development. The Common Pigeon (*Columba livia domestica*) is altricial and the about three times higher density of RGCs in its retina compared to that in Chicken (*Gallus gallus domesticus*), primarily results from a prolonged expansion of the founder neural cell pool and a general delay of neurogenesis (Rodrigues et al., 2016). Our study uncovers that in the OT, in contrast to what happens in the retina, the onset of neurogenesis coincides in Common Pigeon and Chicken. Then, from the 7$^{th}$ day of embryonic development (E7), there are major points of divergences between the two species. In Chicken, tectal cells stop to divide and newborn precursor cells rapidly migrate to establish the different outer layers (e.g., SGFS). In Common Pigeon, neurons differentiate while they get stuck in the ventricular zone (VZ) up to the end of the expansion of a late pool of progenitor cells committed to generate neural cells of the SGFS. Morphological, histological and transcriptomic comparisons of OT development in Common Pigeon and Chicken enabled us to identify elements of a hitherto unknown system deployed by modern birds for increasing neuron densities in the midbrain.

## RESULTS

The results are organized around two main findings about the adaptation of the optic tectum to foveal vision: (1) increased neuron density in the optic tectum of bird species with one or two foveae; (2) consistent with this morphological difference, the development of the optic tectum of foveate and afoveate birds differs dramatically.

### 1. *Interspecies differences of cell densities in the optic tectum of Neoaves and Galloanserae*

Behavioral tests show that birds have the best visual acuity when their retinas possess one or two foveae. The large majority of RGC axons that compose the optic nerve terminate in the SGFS of the OT where they establish connections with neurons in an orderly fashion according to a retinotopic mapping (Figure 1A). We asked whether there was a link between the number and architecture of fovea and the cell density in the SGFS. We selected twelve bird species with one or two foveae or without this retinal specialty. They were from seven taxonomic Orders with varying brain weight up to one order of magnitude (Table S1). Histological analysis of the foveae and cell counting in the OTs were performed on the same specimens. Although all the avian predators we examined have laterally placed eyes, except for the Tawny Owl (*Strix aluco*), they exhibit striking differences in terms of fovea organization (Figure S1, Table S2). The Common Kestrel (*Falco tinnunculus*) has a central and a peripheral fovea, the Northern Goshawk (*Accipiter gentilis*), the Eurasian Sparrowhawk (*Accipiter nisus*) and the Black Kite (*Milvus migrans*) have only a central fovea and a peripheral area with, for some of them, high densities of RGCs and cones, whereas the Tawny Owl has no fovea. The retina of this truly nocturnal species is exclusively populated by rods and the density of RGCs is uniformly low (Figures S1, S2). Although, the Northern Goshawk, the Eurasian Sparrowhawk, the Grey Wagtail (*Motacilla cinerea*) and the Common Pigeon have different feeding habits and foraging behavior, their central fovea looks remarkably similar and none have a peripheral fovea. The Common Swift (*Apus apus*) is among the fastest fliers, catching insects on the wing, yet, its single fovea is situated on the extreme periphery of the retina (Figure S1). To make things even more convoluted, the two swallows studied here, i.e., the Common House-Martin (*Delichon urbicum*) and the Barn Swallow (*Hirundo rustica*) have a central and a peripheral fovea, while their lifestyle and feeding habits are very similar to that of the swifts.

Figure 1

A

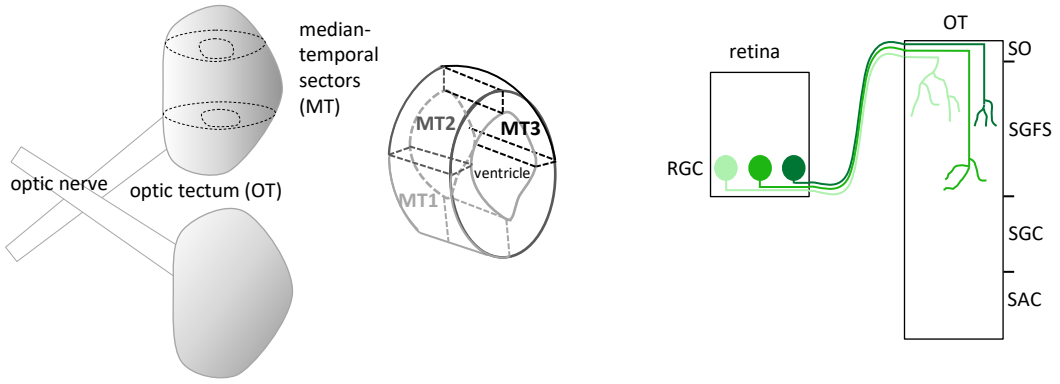
median-
temporal
sectors
(MT)
optic nerve
optic tectum (OT)
MT2
MT3
ventricle
MT1
retina
OT
RGC
SO
SGFS
SGC
SAC

B

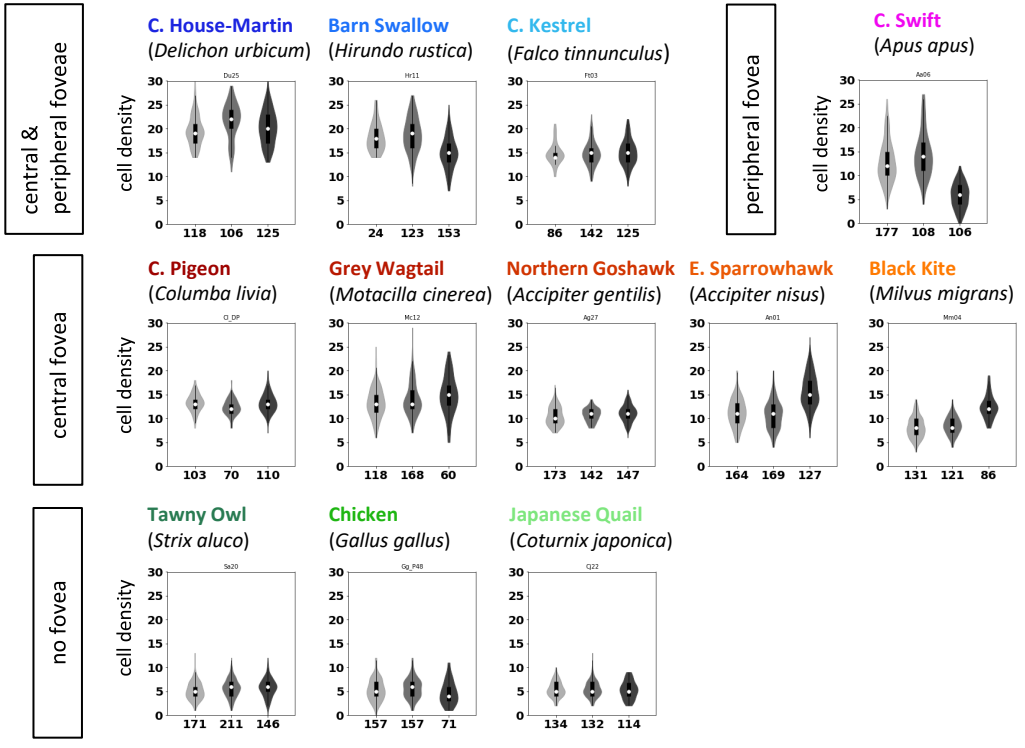
central &
peripheral foveae
C. House-Martin
(Delichon urbicum)
Du25
118 106 125
Barn Swallow
(Hirundo rustica)
Hr11
24 123 153
C. Kestrel
(Falco tinnunculus)
Fn03
86 142 125
peripheral fovea
C. Swift
(Apus apus)
Aa06
177 108 106
central fovea
C. Pigeon
(Columba livia)
Cl_DP
103 70 110
Grey Wagtail
(Motacilla cinerea)
Mc12
118 168 60
Northern Goshawk
(Accipiter gentilis)
Ag27
173 142 147
E. Sparrowhawk
(Accipiter nisus)
An01
164 169 127
Black Kite
(Milvus migrans)
Mm04
131 121 86
no fovea
Tawny Owl
(Strix aluco)
Sa20
171 211 146
Chicken
(Gallus gallus)
Gg_P48
157 157 71
Japanese Quail
(Coturnix japonica)
Cj22
134 132 114
cell density

C

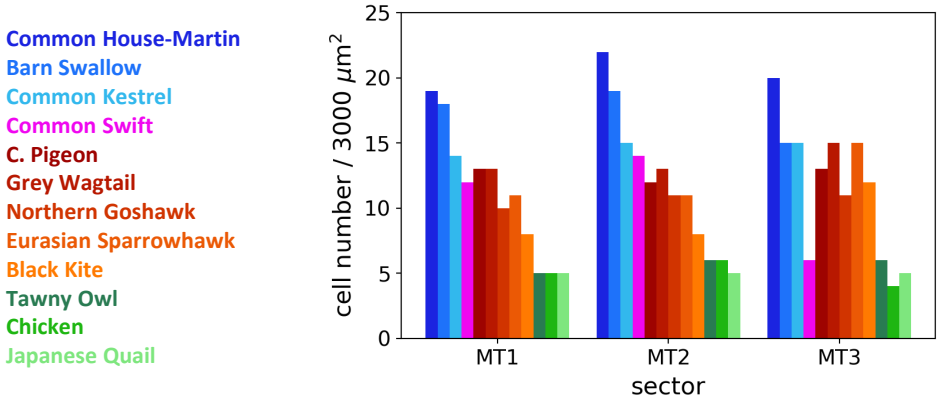
Common House-Martin
Barn Swallow
Common Kestrel
Common Swift
C. Pigeon
Grey Wagtail
Northern Goshawk
Eurasian Sparrowhawk
Black Kite
Tawny Owl
Chicken
Japanese Quail
cell number / 3000 μm²
MT1
MT2
MT3
sector

**Figure 1 - Cell density in the optic tectum.** (A, left panel) the three median-temporal sectors of the optic tectum (OT) selected for cell counting. (A, right panel) Retinal ganglion cells (RGCs) innervate the superficial layers of the OT (SGFS) according to a retinotopic map. SO, stratum opticum, SGFS, stratum griseum et fibrosum superficiale, SGC, stratum griseum centrale, SAC, stratum album centrale. (B) Violin plots showing, for each studied species, the number of cells fitting in 50 µm x 60 µm frames (on the y-axis) used to screen the sectors MT1 (light gray), MT2 (middle gray) and MT3 (dark gray). The cell density is thus defined as the number of cells fitting in such a 3000 µm² counting frame. Values on the x-axis correspond to the number of counting frames used to screen each sector. There is one violin plot per species and per sector. Each violin plot shows the empirical distribution of the cell density obtained with a Gaussian kernel density estimation. Additionally, a more traditional box plot is overlaid: the white dot on each violin plot shows the median, the vertical black bar shows the interquartile range (IQR), whereas the black line shows the range between lower and upper whiskers. Lower (respectively upper) whisker is located at a 1.5 IQR distance measured down (respectively up) from the lower (respectively upper) quartile or at the smallest (respectively largest) data point. The values on the x-axis are the number of data points – i.e., the number of counting frames used to draw each violin plot as well as the overlying box plot. (C) Bar plot showing, for each studied species, the median cell densities (on the y-axis) across the three sectors of the median-temporal domain. The color of each bar is the color identifying the corresponding species.

**Figure S1 - Fovea diversity in birds.** Pictures of semi-thin cross-sections (1 µm thick) of the central and peripheral retinas of the twelve bird specimens investigated in this study (Table S1). All pictures (except the inset and the close-up pictures) are at the same scale. The foveate or afoveate peripheral retinal areas shown here are located in the temporal quadrant. Some basic features of the foveae and cell counts in the GCL and ONL are presented in the Table S2 and the Figure S2. Of special note: (1) While the eye of the Common Kestrel is 2.2 times larger than that of the Barn Swallow (Table S1), the sizes, the deepness and the shape of the central foveae of these two species are identical. (2) In the Common Swift, the only fovea is located in the far periphery, where the retina joins the ciliary marginal zone (CMZ, inset). The pit is deep despite its eccentric position. (3) We did not find differences (e.g., deepness of the fovea, cell density in the GCL and ONL) between captive domestic pigeons and racing (homing) specimens, as well as between 10 weeks (P70) and 6 years old pigeons (our unpublished data). (4) While the eye of the male Northern Goshawk is 1.4 times larger than that of the male European Sparrowhawk (Table S1), the sizes, the deepness and the shapes of the central foveae of these two Accipiter species are identical. (5) The Tawny Owl is the only Neoaves of our collection with no fovea. The photoreceptors of this true nocturnal bird are rods with very long outer segments (PRS). (A-D) Six close-up pictures illustrating special features of bird foveae. (A) The bending of the inner segments of cones lying within the pit (dashed yellow line). The inner segments tend to get aligned with rows of bipolar cells in the INL (dashed red line). (B) Somas of giant RGCs (surface areas ≥100µm2; Figure S2B) on the edge and within the pit of the peripheral fovea. (C) cone photoreceptors identifiable by the presence of an oil droplet in the outer segment (arrowheads). (D) Columnar organization of cells in the GCL is observed on the edges of both deep and shallow central foveae. It is, however, less frequent in peripheral foveae. PRS, outer segment of photoreceptor; ONL, outer nuclear layer; INL, inner nuclear layer; IPL, inner plexiform layer; GCL, ganglion cell layer. Scale bars: 200 µm.

Figure S1

central retina peripheral retina

**Common House-Martin** (*Delichon urbicum*)

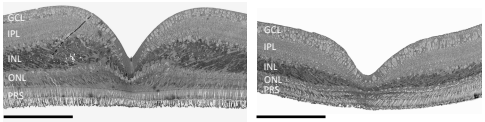


**Barn Swallow** (*Hirundo rustica*)

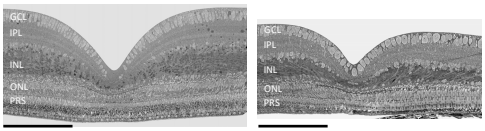


**Common Kestrel** (*Falco tinnunculus*)

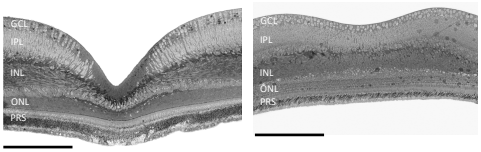


**Common Swift** (*Apus apus*)

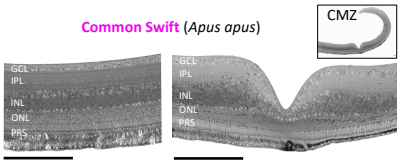


**C. Pigeon** (*Columba livia domestica*)

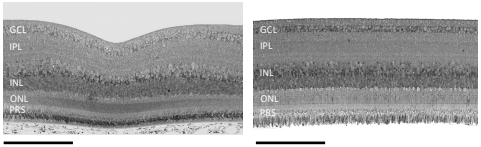


**Grey Wagtail** (*Motacilla cinerea*)

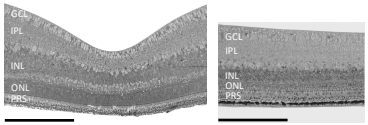


central retina peripheral retina

**Northern Goshawk** (*Accipiter gentilis*)

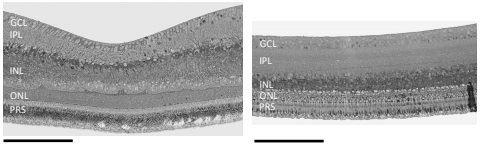


**Eurasian Sparrowhawk** (*Accipiter nisus*)

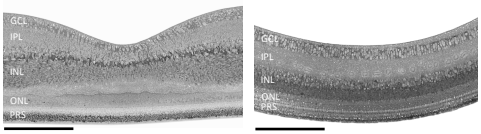


**Black Kite** (*Milvus migrans*)

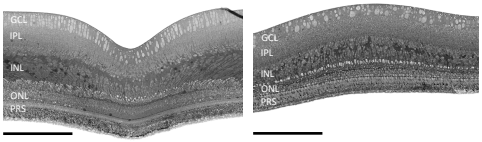


**Tawny Owl** (*Strix aluco*)

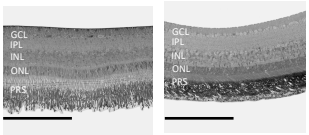


**Chicken** (*Gallus gallus domesticus*)

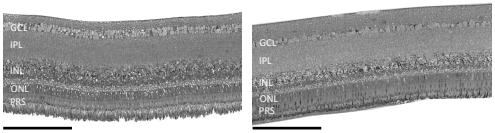


**Japanese Quail** (*Coturnix japonica*)

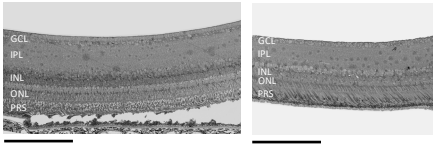


Close-up:

A **C. House-Martin** peripheral fovea

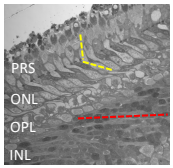


B **Barn Swallow** peripheral fovea

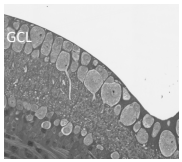


C **Common Swift** peripheral fovea

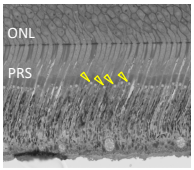


D **Black Kite** central fovea

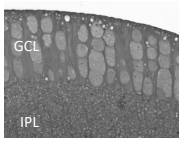


**Common Pigeon** central fovea

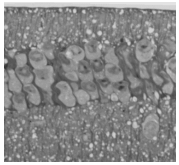

**Barn Swallow** central fovea

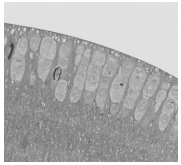

We asked how this diversity in fovea organization reflects on cell densities in the SGFS. The OT lobes were divided in three sectors (MT1, MT2, MT3) that encompassed the whole surface of the OT except the most rostral and caudal parts (Figure 1A). Each sector was sectioned perpendicular to the pial surface. Eight 1 µm-thick sections per sector distributed over a thickness of 200-300 µm were selected. On each section the nuclei with visible nucleoli were counted in 10 to 30 contiguous sectors (50 µm x 60 µm) distributed over the surface of the SGFS (Figure 1B, C). On the whole, in the two representants of Galloanserae and in the Tawny Owl, the cell densities were lower than in diurnal Neoaves. It was in the bifoveate Common House-Martin, Barn Swallow, and Common Kestrel that cell densities reached the highest levels in all of the three sectors. In the MT3 sector, cell densities were higher in Neoaves than in Galloanserae, with the remarkable exception of the Common Swift and Tawny Owl, suggesting that this sector encompasses the central fovea projection area. Likewise, cell densities in the MT1 and MT2 sectors were the highest in the four species with a peripheral fovea, suggesting that the two sectors share the projection area of this fovea. Cell densities in the MT1 and MT2 sectors were still higher in the five foveate species with no peripheral fovea than in afoveate birds. This is consistent with the fact that RGC densities in the peripheral retinas of foveate birds were higher than in afoveate birds (Figure S2). In the Tawny Owl, unlike in foveate Neoaves, cell densities in the sectors MT1, MT2 and MT3 were at the same low levels as in Galloanserae (Figure 1B, C). This result strengthens the idea that increased cell densities in the largest visual center of the brain are related to the presence of one or two foveae rather than changes that may have occurred when birds split between the Galloanserae and Neoaves.

**Table S1 - List of specimens used in the study.**
Abbreviations: nd, not determined; F, female; M, male; J, juvenile; A, adult; Tel, telencephalon; OT, optic tectum; diam, diameter.

| Species | Species (EN) | Age | Sex | Body weight (g) | Brain weight (g) | Eye diam. (mm) | Tel. length (mm) | Tel. width (mm) | Tel. height (mm) | OT length (mm) | OT width (mm) | OT height (mm) | Origin |
|---|---|---|---|---|---|---|---|---|---|---|---|---|---|
| Delichon urbicum | Common house martin | J | nd | 17,33 | 0,49 | 9 | 9 | 7 | 5 | 4 | 2 | 3 | La Vaux-Lierre |
| Hirundo rustica | Barn swallow | J | M | 15,06 | 0,64 | 9 | nd | nd | nd | 5 | 2,5 | 4 | La Vaux-Lierre |
| Falco tinnunculus | Common kestrel | A | M | 158,53 | 3,8 | 20 | 16 | 13 | 10 | 9 | 5 | 7 | La Vaux-Lierre |
| Apus apus | Common swift | A | F | 32 | 0,86 | 12 | 10 | 8 | 6 | 5 | 3 | 4 | La Vaux-Lierre |
| Columba livia | Pigeon | A | nd | 665 | 2,76 | 15,8 | 13,7 | 9,5 | 8,7 | 8,5 | 5,8 | 6,1 | Pigeonneau normand |
| Matocilla cinerea | Grey wagtail | J | nd | 15,73 | 0,65 | 8 | nd | nd | nd | 5,5 | 3 | 4 | La Vaux-Lierre |
| Accipiter gentilis | Northern goshawk | J | M | 776 | 7,96 | 27 | 21 | 18 | 13 | 12 | 7 | 9 | La Vaux-Lierre |
| Accipiter nisus | Eurasian sparrowhawk | A | M | nd | nd | 19 | 15 | 12 | 8 | 9,5 | 5,5 | 7 | La Vaux-Lierre |
| Milvus migrans | Black kite | A | M | 807 | 7,51 | 24 | 19 | 14 | 12 | 10 | 6 | 9 | La Vaux-Lierre |
| Strix aluco | Tawny owl | A | nd | 479 | 9 | 29 | 23 | 18 | 15,5 | 10,5 | 5 | 8,5 | La Vaux-Lierre |
| Gallus gallus | Chicken | A | nd | nd | 3,53 | 21 | 18 | 11 | 10 | 10 | 5 | 7,5 | Fournier |
| Coturnix japonica | Japanese quail | A | F | 324 | 0,86 | 11 | 10 | 7 | 6 | 6,5 | 4 | 5 | Marc Plancherel |

**Table S2 - Comparative analysis of bird specialized areas..**

| Species | Area | Pit | Layer interruption | | |
|---|---|---|---|---|---|
| | | | GCL | INL | ONL |
| Common house martin | central fovea | deep | complete | complete | complete |
| | peripheral fovea | deep | complete | complete | complete |
| Barn swallow | central fovea | deep | complete | complete | partial |
| | peripheral fovea | deep | no | partial | partial |
| Common kestrel | central fovea | deep | complete | complete | partial |
| | peripheral fovea | shallow | partial | no | no |
| Common swift | central area | absent | no | no | no |
| | peripheral fovea | deep | complete | complete | complete |
| Pigeon | central fovea | shallow | no | partial | no |
| | peripheral area | no | no | no | no |
| Grey wagtail | central fovea | shallow | no | partial | no |
| | peripheral area | no | no | no | no |
| Northern goshawk | central fovea | shallow | partial | partial | no |
| | peripheral area | no | no | no | no |
| Eurasian sparrowhawk | central fovea | shallow | partial | partial | no |
| | peripheral area | no | no | no | no |
| Black kite | central fovea | shallow | partial | partial | no |
| | peripheral area | no | no | no | no |
| Tawny owl | central area | no | no | no | no |
| | peripheral area | no | no | no | no |
| Chicken | central area | no | no | no | no |
| | peripheral area | no | no | no | no |
| Japanese quail | centra area | no | no | no | no |
| | peripheral area | no | no | no | no |

### 2. *The main features of the bird fovea*

We found that the cell density in the SGFS of the OT was 2 to 4 times higher in foveate than in afoveate birds. Similar difference was measured between the V1 of primate vs. non-primate mammals (Collins et al., 2010; Rockel et al., 1980; Srinivasan et al., 2015) suggesting that some key features of foveal vision are conserved between diurnal Neoaves and primates. The human fovea is regarded as having the highest spatial resolution of all retinal specializations because of its high density of cones and RGCs and the lowest convergence ratio of cones to RGCs. This allows a concentration of RGCs having small receptive fields, which is presumed to be the substrate for the high acuity pathway. Moreover, in primates, the pit that characterizes the fovea is considered as a way to avoid light scattering by displacing RGCs and interneurons on the rim of the pit as well as to improve the picture that projects on foveal cones by a lens effect.

One common feature of birds with a central fovea is the higher density of RGCs in their central retina and of SGFS neurons in their MT3 sector (Figures 2, S2). As a general trend, densities of photoreceptors, mostly cones, were higher in species with a central fovea. However, there is no central fovea in the Common Swift and the cone density in its central retina is the highest among all species investigated here (Figures S1, S2). Our interspecies comparisons revealed that the relative differences in cell densities between the ganglion cell layer (GCL) and the SGFS varied depending on whether the foveae were deep or shallow (e.g., the comparison between the Common House-Martin and the Northern Goshawk, Figure 2A, B). Likewise, the four species with a peripheral fovea display the highest cells densities in their MT1 and MT2 sectors, while RGC densities within and around their peripheral pit are often lower than in Neoaves with no peripheral fovea (Figures 2, S1, S2). This raises the possibility that a foveal RGC could be connected with a greater number of tectal cells than a RGC outside the fovea, a trend that might be even more pronounced in retinas with a deep fovea.

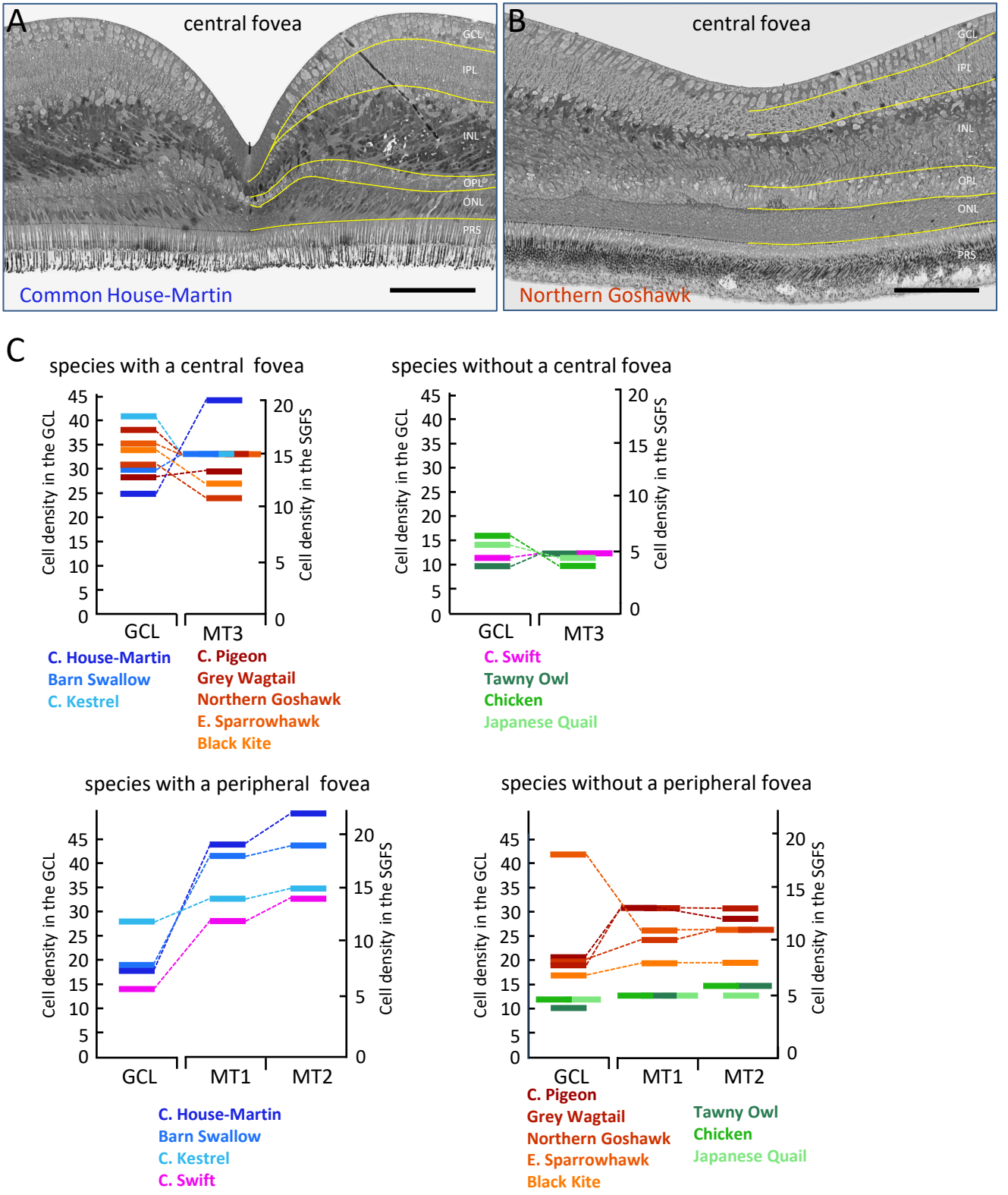
A
central fovea
GCL
IPL
INL
OPL
ONL
PRS
Common House-Martin
B
central fovea
GCL
IPL
INL
OPL
ONL
PRS
Northern Goshawk
C
species with a central fovea
Cell density in the GCL
Cell density in the SGFS
GCL
MT3
C. House-Martin
Barn Swallow
C. Kestrel
C. Pigeon
Grey Wagtail
Northern Goshawk
E. Sparrowhawk
Black Kite
species without a central fovea
Cell density in the GCL
Cell density in the SGFS
GCL
MT3
C. Swift
Tawny Owl
Chicken
Japanese Quail
species with a peripheral fovea
Cell density in the GCL
Cell density in the SGFS
GCL
MT1
MT2
C. House-Martin
Barn Swallow
C. Kestrel
C. Swift
species without a peripheral fovea
Cell density in the GCL
Cell density in the SGFS
GCL
MT1
MT2
C. Pigeon
Grey Wagtail
Northern Goshawk
E. Sparrowhawk
Black Kite
Tawny Owl
Chicken
Japanese Quail

**Figure 2 - Fovea and cell densities in the GCL and the SGFS.** (A, B) Deep vs. shallow foveae. (A) In the deep fovea, the ganglion cell layer (GCL), the inner nuclear layer (INL) and the outer nuclear layer (ONL) are interrupted. The lateral displacement of cells of the INL and ONL leads to the thickening of these layers around the pit. In contrast, the much decreased number of GCL cells within the pit does not result from the displacement of cells on the edge of the pit. (B) In the shallow fovea, there is no layer interruption, but a thinning of the INL. (C) Graphical representations that associate cell densities in the GCL with those in the SGFS (data are from the Figures 1C and S2A). Species with no fovea display the lowest cell densities in the GCL and in the SGFS. In foveate birds, the relative differences in cell densities between the GCL and the SGFS vary depending on whether the fovea is deep or shallow. The Common House- Martin has the deepest central fovea, the cell density in its central GCL is the lowest among the species with a central fovea and the cell density in the SGFS of its MT3 sector is the highest. There is a similar trend in the peripheral retina. The swallow and swift species have the deepest peripheral foveae and the highest cell densities in the SGFS of their MT1 and MT2 sectors. The Common Kestrel has a shallow peripheral fovea and cell densities in the MT1 and MT2 sectors are comparatively lower, while the cell density in its peripheral GCL is the highest among the species with a peripheral fovea. The Eurasian Sparrowhawk has no peripheral fovea. Yet, the cell density in its GCL reaches the highest value of all species, while cell densities in the MT1 and MT2 sectors are among the lowest. Scale bars: 100 µm.

**Figure S2 - Neuron densities in the retina.** (A) Cells in the GCL and ONL were counted on semithin cross-sections (1 µm thick) of the foveal and perifoveal areas (~1 millimeter in length). (A, left panels) Central retina. (A, right panels) Peripheral retina. The orange bars identify the species with a central fovea (left panels) and/or a peripheral fovea (right panels). The species with a central fovea display the highest cell densities in the central GCL. The species with a peripheral fovea are not always the ones that display the highest cell densities in the peripheral GCL. In bifoveate species, cell densities in the GCL are lower in the peripheral fovea than in the central one. The Common Swift has no central fovea, but it displays the highest cell density in the central ONL. Apart from this remarkable exception, cell densities in the ONL are higher in birds with a central fovea. Cell densities are lower in the peripheral ONL than in the central one, except in the Tawny Owl. Cell densities in the peripheral ONL are sometimes lower in species with a peripheral fovea than in species without it. (A, left and right lower panels) In the 12 studied species, the ratios of GCL to ONL cell densities could vary by one order of magnitude. The ratios are < 0.2 in the swift or owl central retinas, while they are equal or close to 1 in the hawk's peripheral retinas. In 10 out of the 12 central and peripheral foveae examined, the ratios are comprised between 0.4 and 0.6. (B, left panel) Central retina. (B, right panel) Peripheral retina. Each violin plot shows the empirical distribution of the soma surface in the GCL obtained with a gaussian kernel density estimation. On the overlaid box plot, the white dot on each violin plot shows the median, the vertical black bar shows the interquartile range (IQR), whereas the black line shows the range between lower and upper whiskers. Note the high proportion of giant cells (29% ≥ 100 µm2) in the peripheral fovea of the Barn Swallow (Figure S1, close-up B).

Figure S2

A

central retina

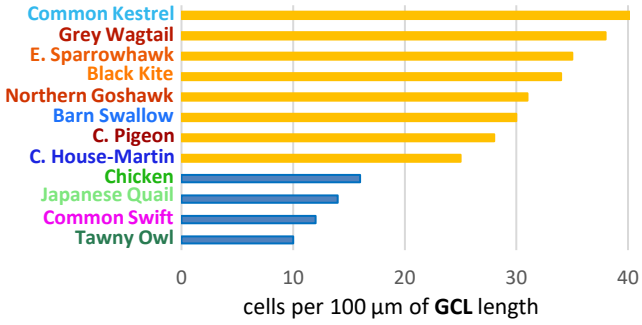


peripheral retina

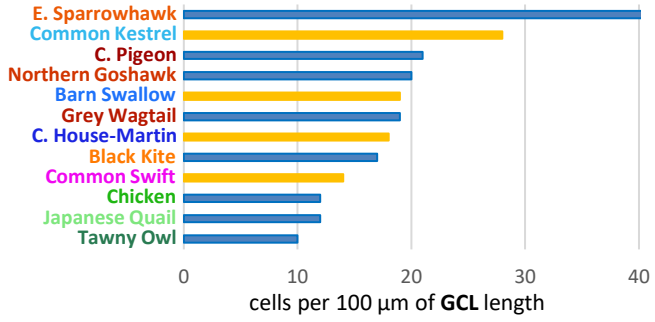


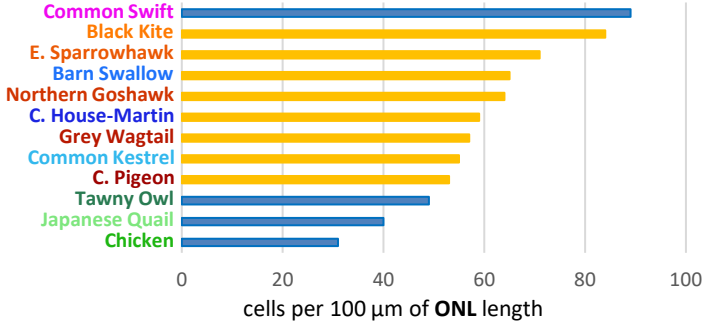


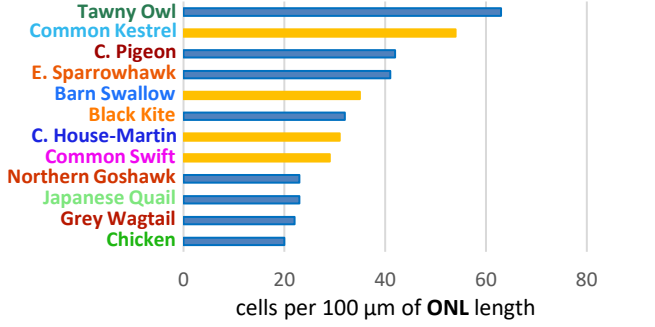


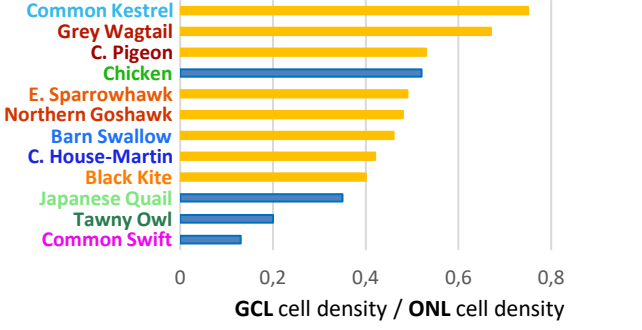


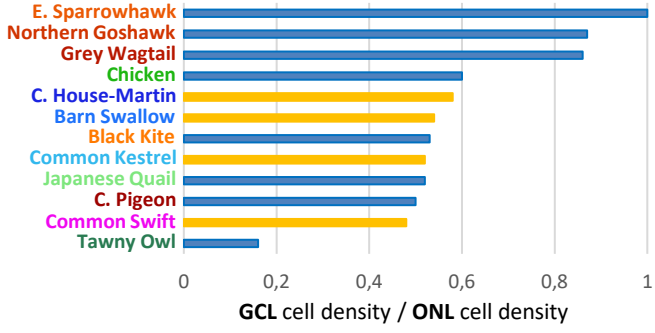


B

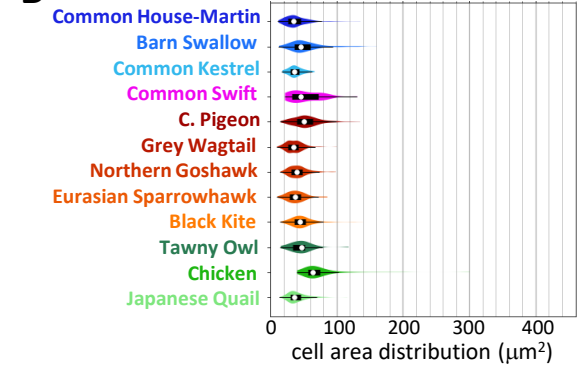


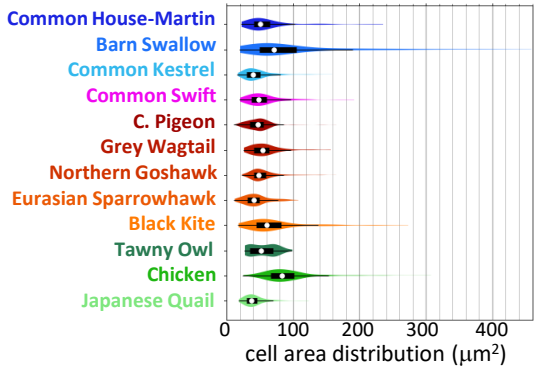

### *3. The incipient fovea in the embryonic retina*

The pit is the most evident feature of the fovea and its formation likely represents the last step in the morphological development of the fovea, which, in human, is completed one year after birth. In Common Pigeon (herein called 'pigeon'), we did observe a fully developed pit eight weeks after hatching. Little is known about the developmental processes that precede pit formation. In pigeon, RGC production is completed around embryonic day 12 (E12). At this stage, the retina is about half of the adult size (~110 $mm^2$ at E12 versus ~250 $mm^2$ 1 year post hatching) and the density of RGCs was high across the retina (60-80 cells per 100 µm, Figure S3; (Rodrigues et al., 2016)). Axon growth contributed to the thickening of the nerve fiber layer (NFL) and to the stretching of the retina afterwards. The expansion of the retina from E12 to adulthood led to a ~5-fold decrease of cell density in the GCL except in a central area of ~450 µm in diameter (Figure S3). The fact that the NFL was much thinner in the central area suggests that RGC axons growing towards the head of the optic nerve largely avoided this central area that we define as the incipient fovea. Its size was unchanged from E12 up to 8 weeks post-hatching. However, cell density in the GCL of the incipient fovea was reduced by half 12 days post-hatching (P12), thereby reaching values measured in the fovea at the adult stage (28 cells per 100 µm; Figures S2, S3). It is worth mentioning that the decrease in cell density at P12 correlated with a bending of the retina in the middle of the incipient fovea (Figure S3). In this perspective, it would be interesting to know whether the decrease of cell density initiates the pit formation and whether it is more pronounced in species with a deep fovea. Future studies should also determine whether decreased cell density results from targeted apoptosis.

Figure S3

E12

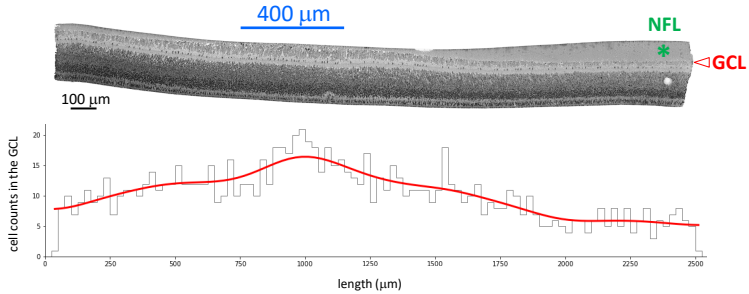


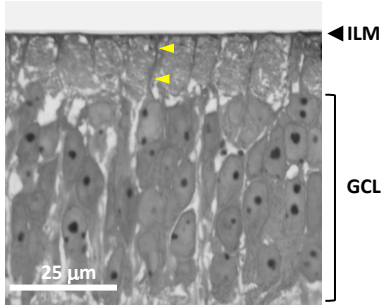


E16

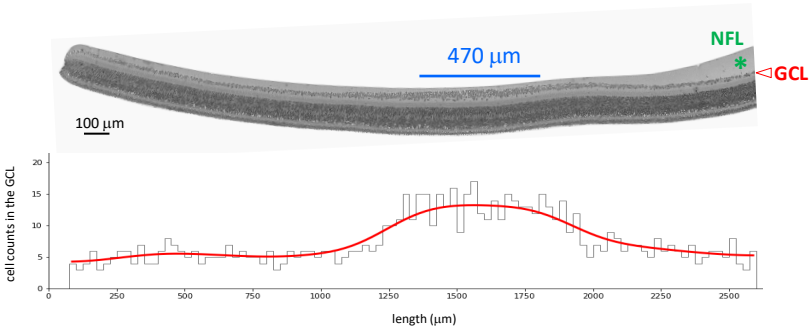


P12

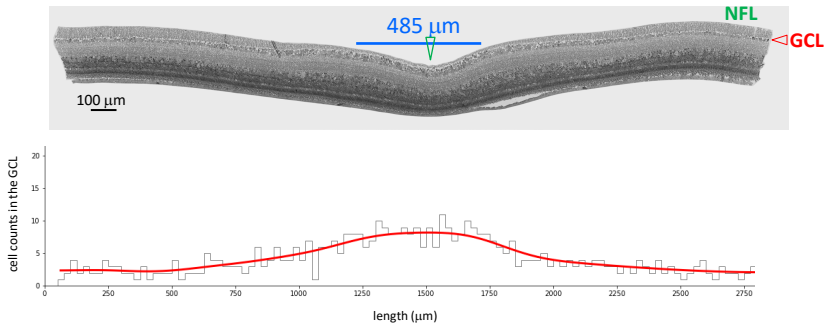


P56

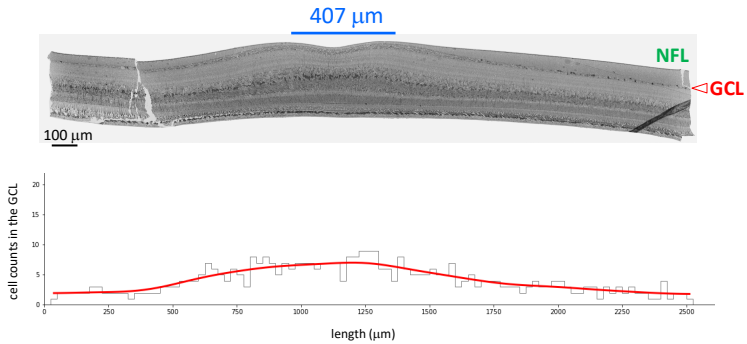

**Figure S3 - The incipient fovea in the developing pigeon retina.** Microphotographs of semi-thin cross-sections (1 µm thick) of the central retina on the 12th (E12) and 16th (E16) day of embryonic development and on the 12th (P12) and 56th (P56) day of development after birth. The blue line delimits the region of higher cell densities in the GCL, which we define as the incipient fovea. The size of this region remains fairly constant from E12 up to P56. The nerve fiber layer (NFL), which is made of RGC axons, is absent (E12) or much thinner (E16, P12, P56) in the incipient fovea. A close-up of this area at E12 shows cells of the GCL abutting the inner limiting membrane (ILM). The plots show cell densities in the GCL. The gray contour corresponds to the number of cells (on y-axis) in vertical frames partitioning the whole section (on x-axis), each one of them having a width of 25 µm. The red curve is obtained by smoothing the binned values with a gaussian kernel with a standard deviation of 5. The average cell numbers per 100 µm retinal length in the incipient fovea are 57 at E12, 50 at E16, 29 at P12, 31 at P56, 28 at P70 (Figure S2). At P12, there is a bending of the retina on the middle of the incipient fovea (green arrowhead) and a ~2-fold decrease of cell density.

### 4. *Difference in cell densities between Neoaves and Galloanserae is achieved during embryogenesis*

Increased density of tectal neurons in bird species with one or two foveae might represent a breakthrough innovation in visual system evolution. Our cross-species comparison indicates that the pigeon is representative of foveate birds, making comparison between pigeon and chicken an appropriate model to ask how the OT had adapted for receiving higher numbers of retinal inputs. Few days before hatching (E14-E17), the size (length, width, thickness) and the estimated volume of the pigeon OT were, respectively, 1.25 (± 0.1) and ~2 times smaller than in chicken (Figure 3A, D). In pigeon, the SGFS layers receive three times more RGC axons than those of chicken at E17 (Figure 3B; Rodrigues et al. (2016)). The stratum opticum (SO) is the most superficial layer of the tectum and it is formed by RGC axons of the optic tract. At E14, the SO was thicker in pigeon than in chicken all along the medio-lateral or the rostro-caudal axis (Figure 3D and data not shown). From E14 through E17 (P0), we noted several histoarchitecture differences between the pigeon and the chicken. At E14, in the chicken OT, LaVail and Cowan (1971a) identified on 20 µm thick paraffin sections 10 layers, numbered i-x from the ependymal surface. On 1 µm thick plastic sections, the cellular layers iv, vi, viii and x were clearly visible in pigeon, whereas they were blurry in chicken, because of the lower cell density (Figure 3D). Cell counting revealed that neuron densities in the layers vi to x were 2 to 4 times higher in pigeon than in chicken at E14 (Figure 3D, E, F). At this stage, the total number of tectal cells was actually the same in pigeon and chicken (Table S3). However, in pigeon, cells were packed in a volume twice smaller. Difference in neuron densities between the pigeon and chicken outer layers exceeded those measured in isotropic suspensions of cell nuclei, reflecting non-uniform scaling with comparatively higher cell densities in the outer laminae where RGC axons terminate. Likewise, at the adult stage, the 2.5 (MT1), 2.2 (MT2), 2.8 (MT3) times higher cell densities in pigeon compared to chicken (Figure 1C) mainly concern cells localized in the superficial layers of the SGFS (Figure 3C). Taken together, our data indicate that the difference in cell density between the pigeon and the chicken are already established at E14.

Figure 3

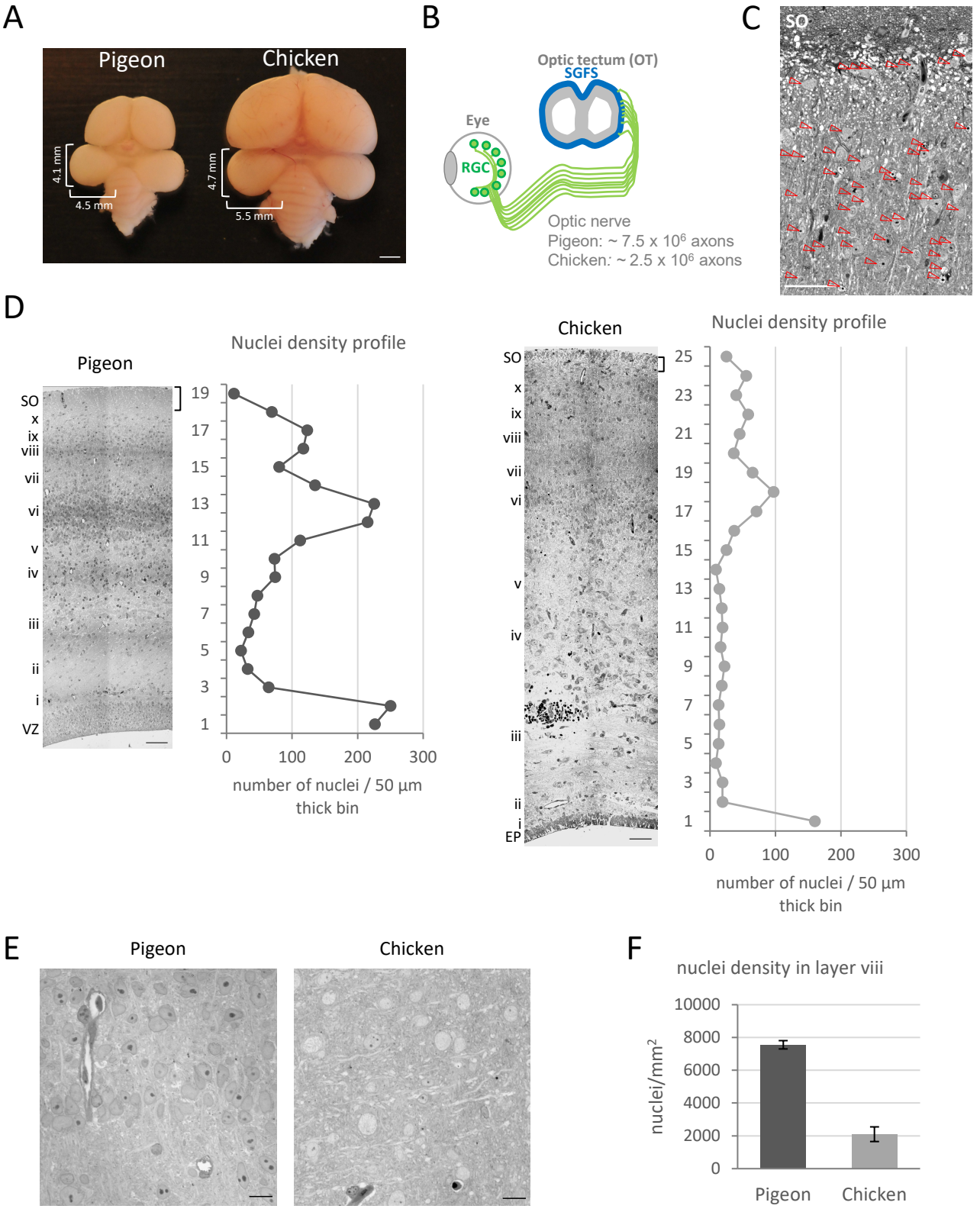
A
Pigeon
Chicken
4.1 mm
4.5 mm
4.7 mm
5.5 mm
B
Optic tectum (OT)
SGFS
Eye
RGC
Optic nerve
Pigeon: ~ 7.5 x 10^6 axons
Chicken: ~ 2.5 x 10^6 axons
C
SO
D
Pigeon
Nuclei density profile
SO
x
ix
viii
vii
vi
v
iv
iii
ii
i
VZ
number of nuclei / 50 µm thick bin
Chicken
Nuclei density profile
EP
number of nuclei / 50 µm thick bin
E
Pigeon
Chicken
F
nuclei density in layer viii
nuclei/mm²
Pigeon
Chicken

**Figure 3 - Cell density patterns in the developing pigeon and chicken OTs.** (A) Pigeon and chicken brain at E17. (B) RGCs make direct connections with SGFS neurons. The number of axons in the optic nerve is ~3 times higher in pigeon than in chicken (Rodrigues et al., 2016). (C) Semi-thin cross-section (1 µm thick) through the outer layers of the SGFS in the MT3 sector of an adult (P70) pigeon. Nuclei are indicated by arrowheads. (D, left panels) Semi-thin sections (1 µm thick) cut radially through a pigeon or a chicken OT at E14. The layers recognizable at this stage are numbered in sequence from the ventricular zone (VZ, in pigeon) or the ependymal surface (EP, in chicken) and the outward according to the convention established by LaVail and Cowan (1971a). The square brackets delimit the stratum opticum (SO). (D, right panels) The middle gray (pigeon) and light gray (chicken) lines show the number of cells (on x-axis) in horizontal frames partitioning the whole section (on y-axis), each one having 50 µm in width. (E) Close-up pictures of the layer viii. (F) Nuclei densities in the layer viii. Scale bars: 2 mm (A), 50 µm (C, D), 10 µm (E).

**Table S3 - Cell counts obtained with isotropic suspensions of tectal cell nuclei.** The values correspond to the total number of nuclei in the two lobes. For each embryonic stage, 3 to 4 embryos were processed separately.

| | | E3 | E4 | E5 | E6 | E7 | E8 | E9 | E10 | E11 | E12 | E13 | E14 | E15 |
|---|---|---|---|---|---|---|---|---|---|---|---|---|---|---|
| Chicken | cell number | 843 667 | 2 643 333 | 8 313 333 | 26 495 000 | 39 061 250 | 44 398 333 | 42 945 000 | 47 667 500 | 45 539 000 | 45 809 000 | 45 236 667 | 44 003 333 | 45 300 000 |
| | stdev | 240666,44 | 684855,22 | 938580,49 | 3599161,9 | 4536254,7 | 2505944,6 | 2966315,1 | 265835,95 | 2124474,8 | 483996,9 | 2973589,3 | 1231273,1 | 2219797,3 |
| | divisions in 24h | n/a | 1,6 | 1,7 | 1,7 | 0,6 | 0,2 | 0 | 0,2 | 0 | 0,0 | 0 | 0 | 0,0 |
| Pigeon | cell number | 485 140 | 888 133 | 1 979 250 | 7 173 333 | 17 790 000 | 26 900 000 | 34 348 333 | 35 620 000 | 40 593 333 | 39 698 333 | 41 680 000 | 47 423 333 | 44 023 125 |
| | stdev | 115390,2 | 92606,983 | 391478,71 | 2904140,7 | 2721635,5 | 1317725,3 | 1551856,4 | 3267292,5 | 3371977,7 | 3696729,4 | 3974295 | 1875535,5 | 3452338,2 |
| | divisions in 24h | n/a | 0,9 | 1,2 | 1,9 | 1,3 | 0,6 | 0,4 | 0,1 | 0,2 | 0 | 0,1 | 0,2 | 0 |

### *5. The onset of neurogenesis in the pigeon and chicken optic tectum*

Like other altricial birds, the pigeon hatches with closed eyes. We wondered whether the prolonged OT development after birth (Bagnoli et al., 1987; Manns and Gunturkun, 1997) could result from delayed neurogenesis. To answer this point, we first compared how neurogenesis unfolds in the pigeon and chicken OTs at early stages of embryonic development. Measuring the sizes, the number of cells and the number of cell division per day indicated that the pigeon and chick OTs grew and expanded at a similar pace from E3 to E6 (Figure 4A; Table S3). Monitoring Ngn2 expression revealed that neurogenesis peaked between E6 and E7 in both species (Figure 4C). NeuroD4 (formerly named NeuroM) marks OT cells at the time of birth and when they are located in a zone immediately superficial to the neuroepithelium (Roztocil et al., 1997). NeuroD4 transcript accumulated according to similar kinetics in pigeon and chicken suggesting that cell birth and the onset of neuronal differentiation follow the same trend (Figure 4C). This is also reflected in the fact that axon growth was detected from E5 in both species (Figure 4D). Until E6, the pigeon OT had the form of a thin-walled vesicle consisting of an ependymal zone layered with neural epithelial cells and newborn neurons defining the ventricular zone (VZ) and an outer layer formed by a meshwork of radial fibers (Figure 4B). The ~3-fold increase in cell numbers measured in both species between E5 and E6 (Table S3) did not lead to an increase of epithelium thickness but rather resulted in the whole tangential expansion of the tectal tissue (Figure 4A). At E6, we noticed that cells had already started to migrate between glial fibers in chicken, whereas that was not yet the case in pigeon (Figure 4B). At this stage, we had no evidence that the onset of neurogenesis was delayed in the pigeon OT, in contrast to what happens in the retina (Rodrigues et al., 2016).

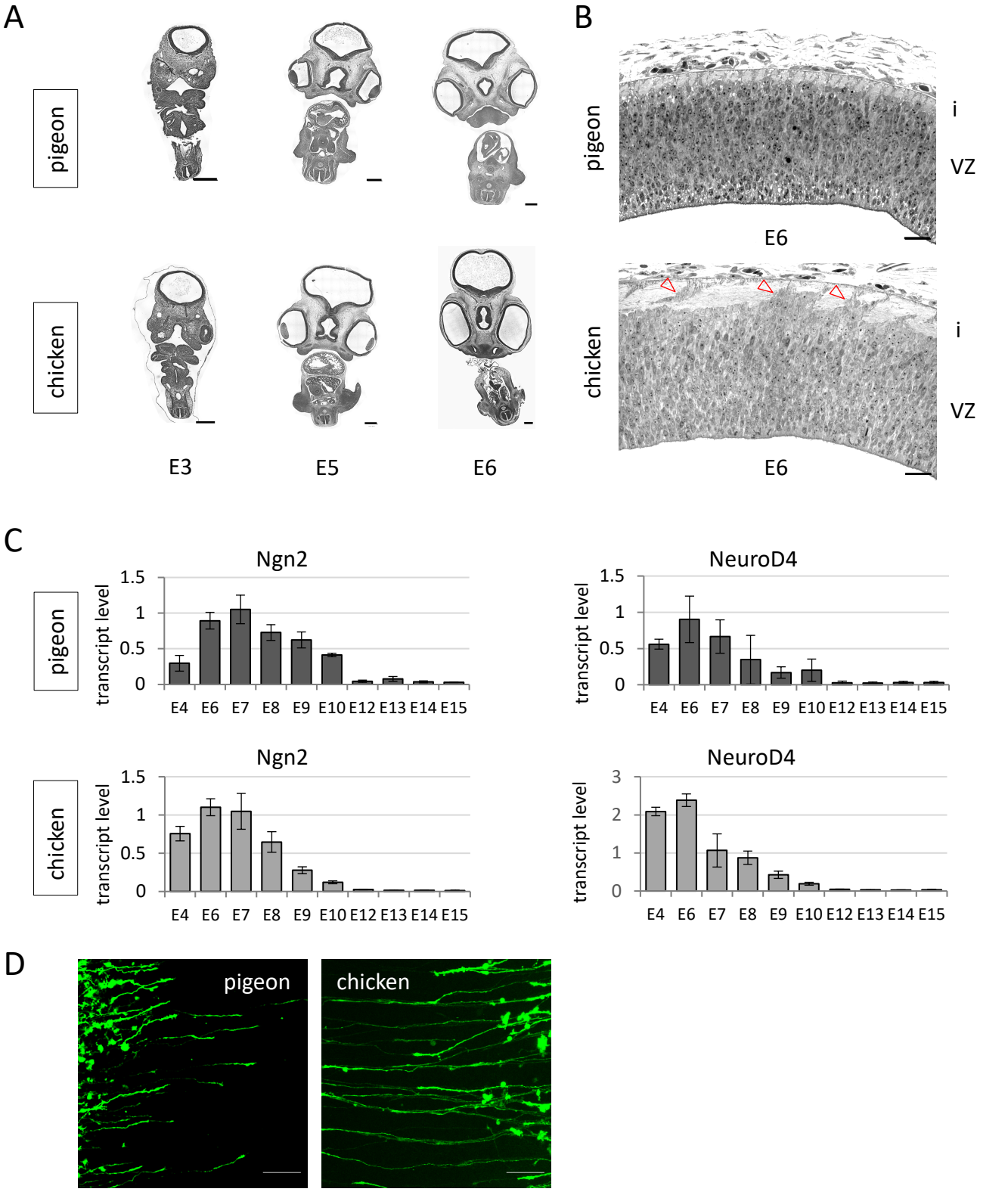
A
pigeon
chicken
E3
E5
E6
B
pigeon
chicken
i
VZ
E6
C
Ngn2
NeuroD4
transcript level
E4 E6 E7 E8 E9 E10 E12 E13 E14 E15
D
pigeon
chicken

**Figure 4 - Early development stages of the pigeon and chicken OT.** (A) Frontal sections through the whole embryo at the level of the midbrain. The OT vesicles are on the top of the pictures. (B) Semi-thin cross-sections (1 µm thick) of the central portion of the OT, i.e., midway between its dorsomedial and ventrolateral borders. Superficial to the VZ lies the outer glial fibers (layer i). The arrowheads in chicken OT point to cells positioned between glial fibers. (C) Accumulation of Ngn2 and NeuroD4 (NeuroM) transcripts measured by RT-qPCR analysis. At each developmental stage, data are from three biological replicates and presented as the mean ± s.d. (D) Pigeon and chicken OT were electroporated in ovo with a Hes5.3-GFP reporter plasmid at E4.5. Labelled axons were visualized 24 hours later. Scale bars: 500 µm (A), 25 µm (B), 50 µm (B).

### 6. *Interspecies divergence of developmental trajectories*

On the 7th day of embryonic development, the pigeon and chicken OTs displayed similar radial glia fascicles consisting of equally spaced parallel thick rows of glial fibers abutting the VZ (Figure 5A, B; Gray and Sanes (1991)). However, whereas in chicken cells arranged in single files migrate along glial fibers to form the tectal plate, in pigeon no cell filled the fascicle interspaces and the tectal plate did not form. The deepening of the groove separating the right and left optic lobes proceeded at a fast pace in chicken, whereas the two lobes did not separate in pigeon. In chicken, most cells were born at E7 (Figure 6A, Table S3) and the lamination led to a rapid thickening of the OT. In contrast, in pigeon, there was no cell migration out of the VZ between E7 and E9 (Figure 5A, B). To investigate further the significance of these striking cross-species differences, we compared in pigeon the development periods that extended from E6 to E7 and from E7 to E9 (Figure S4). The number of cells doubled during each of these periods. The 3D reconstruction of the OT with 10 µm thick serial sections showed that the tissue volume increased 2-folds from E6 to E7 and 2.5-folds from E7 to E9. However, the growth pattern of the tissue had drastically changed over the E6 to E9 period of development. Between E6 to E7, the tissue expanded tangentially and its length along the rostro-caudal axis increased, while the thickness of the tectal tissue and the number of cells in radial columns remained basically constant. This stands in sharp contrast to what happened from E7 to E9. During this latter period, there was no tangential growth along the rostro-caudal axis, whereas there was a marked thickening of the tissue and the number of cells in radial columns encompassing the VZ increased by ~60% (Figure S4). Our histological and morphometric analysis suggest that late cell division in the pigeon happens in a cellular environment different to that prevailing up to E7. Late cell proliferation in a VZ expanding radially - i.e., almost exclusively along its apicobasal axis - led to an increase in the number of cells in radial columns, thereby setting the condition for an increase of cell density. This model of tissue morphogenesis raises a number of questions about the status of cells stuck in the thickened VZ abutting the glial scaffold (Figure 5C).

Figure 5

A

Pigeon

Chicken

E7

E9

i

VZ

ii

ix

vii-viii

v-vi

iv

B

Pigeon E7

Chicken E7

C

radial glia
fascicles
(layer i)

VZ

late progenitor cell

neuron

neural precursor

radial glia

**Figure 5 - Divergent development of the OT between pigeon and chicken.** (A, left panels) Low magnification pictures of frontal sections through the OT. (A, right panels) Semi-thin cross-sections (1 µm thick) of the central OT, i.e., midway between its dorsomedial and ventrolateral borders. At E7, the thicknesses of the VZ are the same in pigeon and chicken. From E7 to E9, VZ thickness increases by ~40% in pigeon, whereas it decreases by ~45% in chicken. At E9, the VZ is ~2.5 times thicker in pigeon than in chicken. In chicken, at E7, cells arranged in single files (arrowheads) migrate along glial fibers (layer i) and form the outer layer ii; at E9, the wall of the tectum has increased in width and 9 layers (i-ix) can be identified. In pigeon, at E7 and E9, the two lobes do not yet separate and the width of the OT remains basically unchanged. Rare cells are scattered in the layer i, but none of them did cross this layer. (B) Semi-thin sections (1 µm) cut tangentially through the fiber layer i of pigeon and chicken OT at E7. In chicken, rows of cell-rich and fiber-rich stripes alternate, whereas in pigeon, there is no cell between the fiber-rich stripes. (C) The diagram outlines the situation in the pigeon OT from E7 to E9. The organization of the VZ is based on data presented in the Figures 6 and 7. Scale bars: 500 µm (A, heads), 50 µm (A, OT sections; B), 5 µm (B, close-up pictures).

**Figure S4 - Morphometric measurement of the developing pigeon OT.** Cell counts data were obtained from isotropic suspensions of cell nuclei (Table S3). Tissue volume data are from the 3D reconstruction of the OT with serial cross-sections (10 µm thick). The rostro-caudal length corresponds to the sum of the 10 µm thick serial cross-sections. The height of the radial columns corresponds to the distance (thickness) between the ventricular and the outer surfaces measured on central sections. Cells per radial column correspond to the number of nuclei counted on semi-thin cross-sections (1 µm thick) in 50 µm wide sectors.

Figure S4

# Pigeon optic tectum

| | E6 | E7 | E9 |
|---|---|---|---|
| cell counts | $7.17 \times 10^6$ | $17.79 \times 10^6$ | $34.33 \times 10^6$ |
| tissue volume | 1.02 $mm^3$ | 1.91 $mm^3$ | 5.15 $mm^3$ |
| rostro-caudal length | 1.68 mm | 2,30 mm | 2,13 mm |

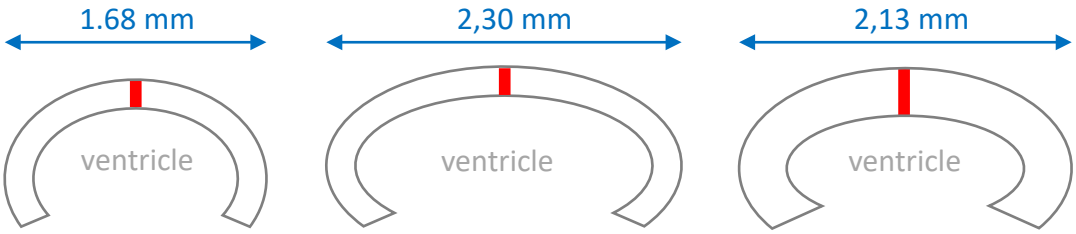


| | | | |
|---|---|---|---|
| radial column | | | |
| height (μm): | 160±10 | 178±11 | 288±15 |
| width (μm): | 50 | 50 | 50 |
| nuclei/radial column: | 90±7 | 95±8 | 153±12 |

### *7. Late progenitor cells divide in a radially expanding ventricular zone*

In pigeon, at E7, the number of OT cells was at ~50% of the maximum (Figure 6A). When E8 or E9 OT explants were pulse-labelled with BrdU for 1 hour, labelled cells were abundant all over the dorsoventral surface of the tectum (Figure 6C). More than 95% of labelled cells were localized on the apical side of the VZ, whereas very few were found on the basal side abutting radial glia (Figure 6D). Cells of the VZ were tightly packed and their distribution looked quite homogeneous (Figure 5A). To estimate the fraction of cells that still proliferate, E7, E8 and E9 OT explants were incubated with BrdU for 19 hours. Dissociated cells were plated on slides and processed for immunodetection (Figure 6E, F). The proportions of labelled cells suggest that a pool of progenitor cells corresponding to ~28% of the total number of cells divided between E7 and E8, and that another pool of similar size divided again between E8 and E9. The much decreased number of labelled cells detected between E9 and E10 suggests that the period of prolonged cell proliferation was completed shortly after E10. Hes5.3 is expressed in progenitor cells during the penultimate and last cell cycle (Chiodini et al., 2013). In pigeon, Hes5.3 transcript level remained close to its peak value up to E9, whereas it rapidly decreased in chicken after E6 (Figure 6B).

Figure 6

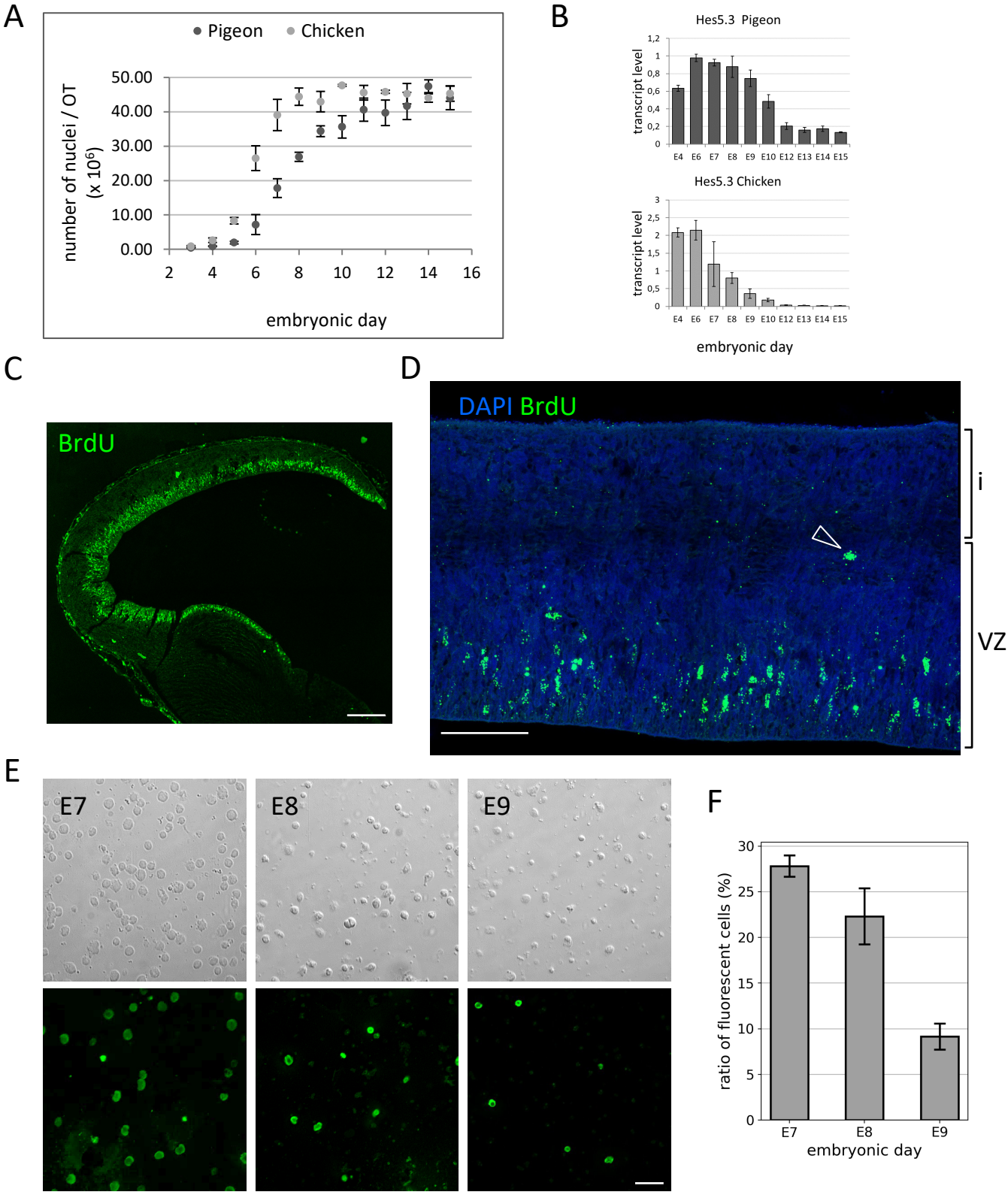
A
Pigeon
Chicken
number of nuclei / OT (x 10^6)
50.00
40.00
30.00
20.00
10.00
0.00
2
4
6
8
10
12
14
16
embryonic day
B
Hes5.3 Pigeon
transcript level
1,2
1
0,8
0,6
0,4
0,2
0
E4 E6 E7 E8 E9 E10 E12 E13 E14 E15
Hes5.3 Chicken
transcript level
3
2,5
2
1,5
1
0,5
0
E4 E6 E7 E8 E9 E10 E12 E13 E14 E15
embryonic day
C
BrdU
D
DAPI BrdU
i
VZ
E
E7
E8
E9
F
ratio of fluorescent cells (%)
30
25
20
15
10
5
0
E7
E8
E9
embryonic day

**Figure 6 - Late cell proliferation in the pigeon OT. (**A) Cell counts obtained with isotropic suspensions of tectal cell nuclei (see also Table S3). For each embryonic stage, 3 to 4 embryos were processed separately. Data are presented as mean ± s.d. (B) Accumulation of Hes5.3 transcripts measured by RT-qPCR analysis. At each developmental stage, data are from three biological replicates and presented as mean ± s.d. (C-F) BrdU pulse-labelling experiments. OTs were dissected at E8 (C) or E9 (D) and incubated as explants with BrdU for 1 hour. After a 1 hour chase, the tissues were fixed and embedded in paraffin. Sections were processed for immunohistochemistry (C, D) and counterstained with DAPI (D). (D) > 95% of labelled cells are localized on the apical side of the VZ. Rare cells (e.g., the one indicated by the arrowhead) are detected on the basal side of the VZ. (E, F) OTs were dissected at E7, E8 or E9 and incubated as explants with BrdU for 19 hours. Dissociated cells were processed for immunohistochemistry. (E) Phase-contrast and fluorescence images are shown. (F) Percentage of BrdU-labelled cells. Data are from three independent experiments and are presented as mean ± s.d. Scale bars: 200 µm (C), 50 µm (D), 20 µm (E).

### 8. *In pigeon, different genes regulate proliferation of the early and of the late progenitor cells*

In pigeon, the late cell proliferation (E7 to E10) occurred in a cellular context different from the one that prevailed up to E7. To analyze molecular features of OT cells, we compared the diversity of the pigeon and chicken RNA-Seq transcriptomes at E6, E8 and E10. In chicken, we anticipated that DNA replication, cell cycle progression and mitosis would be one of the major source of transcriptional variations between E6 and E8 because the large majority of cells have stopped to divide at E7 (Figure 6A; LaVail and Cowan (1971b). Indeed, 97 genes involved in cell proliferation were downregulated in chicken during this period (Figure 7A). In pigeon, the situation was highly contrasted and we split the set of 97 genes into three subsets: 1) 62 genes displayed no significant change of expression between E6 and E10; 2) 22 genes that initiate DNA replication like those encoding the ORC1 and MCM5 subunits or those representing G1 and G1/S checkpoint like CCND1, CDKN3, CDCA7, CKS2 were downregulated in pigeon between E6 and E8, much like in chicken; 3) quite surprisingly, 13 genes were specifically upregulated in pigeon between E6 and E8, and, for some of them, between E8 and E10. For example, the gene POLE that encodes the central catalytic subunit of the DNA polymerase epsilon was strongly upregulated during the two periods in pigeon (+3.24 E6-E8; +1.92 E8-E10 in log2), whereas it was downregulated in chicken (-1.43 E6-E8; -0.50 E8-E10 in log2). On the other side, ORC1 was strongly downregulated both in pigeon (-4,88 in log2) and in chicken (-2,53 in log2) between E6 and E8, whereas the expression of ORC2-6 did not vary in pigeon during this period. ORC1-6 binds to origins of replication as a ring-shaped heterohexamer and the subunit ratios could vary (Shibata et al., 2016). Likewise, the ratios of ORC subunits might differ between early and late pigeon progenitor cells. Another major interspecies difference was that genes representing G2/M checkpoint like CCNB2, TICRR or key steps in cellular response to DNA damage like ATR, FANCL, MCPH1 (microcephalin), NDE1 and TSN (translin) were strongly activated in pigeon between E6 and E8 (e.g., +3,77 for TSN; +3.39 for MCPH1 in log2), whereas they were downregulated in chicken (-1.10 for TSN; -2.17 for MCPH1 in log2). Mutation or ablation of ATR, MCPH1 or NDE1 in mice induce brain malformations (Feng and Walsh, 2004; Gruber et al., 2011; Lang et al., 2016; Lee et al., 2012). In pigeon, the vast majority of late progenitors generate neural cells of the SGFS (see section *Fate and positioning of cells produced by the late pool of progenitors*). The late upregulation of genes controlling proliferation (and, for some of them, genome stability) could be a feature of progenitors that generate neural cells of the SGFS. However, the fact that in chicken these genes were already downregulated when progenitors that generate neural cells of the upper layers of the OT were still proliferating (Figure 7A; LaVail and Cowan (1971b)) argues against this idea. We would suggest that these genes are

specifically activated in pigeon in response to extrinsic conditions that may prevail in the VZ from E7 to E10 (Figure 5C; e.g., the environmental stress resulting from neurons-progenitor cell proximity).

### *9. Neurons differentiate while they remain stuck in the ventricular zone*

Out of the 166 genes that were upregulated in both the pigeon and chicken OT between E6 and E8 and between E8 and E10, 72 are involved in neuronal differentiation and neuronal activity. This set includes 27 genes that regulate axonal and dendritic outgrowth, 21 genes that encode receptors and ion channels and 17 genes involved in synaptogenesis and synaptic transmission (Figure 7A). It is important to remember that genes regulating neuron differentiation in pigeon from E6 to E8 were exclusively expressed by cells residing in the VZ (Figure 5A). Gene expression profiling in the developing brain of birds is still in its infancy. However, it is well established that cholinergic circuits are involved in the visual information processing (reviewed in Knudsen (2011)) and that both SGFS neurons and axon terminals of RGC afferents express nicotinic cholinergic receptors (King, 1990; Matter et al., 1990; Titmus et al., 1999). The neuronal acetylcholine receptor subunit beta-2 (Chrnb2, formerly named non-alpha nAChR) is predominantly expressed in the SGFS (Matter et al., 1990). Chrnb2 transcript steadily accumulated between E4 and E12 both in pigeon and chicken (Figure 7B). However, while transcript level reached a plateau in chicken at E12, it was still increasing in pigeon at E15. NeuroD1 is a regulator of neuron differentiation in the avian nervous system (Matter-Sadzinski et al., 2001; Roztocil et al., 1997) and the expression patterns of this gene were similar in pigeon and chicken until E12. Then, NeuroD1 was rapidly downregulated in chicken, whereas, in pigeon, expression was maintained at high levels at least until E15 (Figure 7B), indicating that neuron production was extended over several days. Axon growth in the pigeon OT was first detected at E5 (Figure 4D). When Hes5.3-GFP and CMV-RFP reporters were co-electroporated in the OT at E4, regularly spaced parallel bundles of GFP-positive axons were detected at E7 (Figure 7C). Bundle thickness (5-10 µm) suggests that axons were growing between the rows of glial fibers (Figure 5B) but close to the VZ as evidenced by the presence of GFP- and/or RFP-labelled cells. Taken together, our data suggest that neural differentiation unfolded at a similar pace in pigeon and chicken. The fact that in pigeon, neurons differentiated while their somas were immobilized in the VZ is likely to challenge our current understanding of how a laminated brain structure develops.

Figure 7

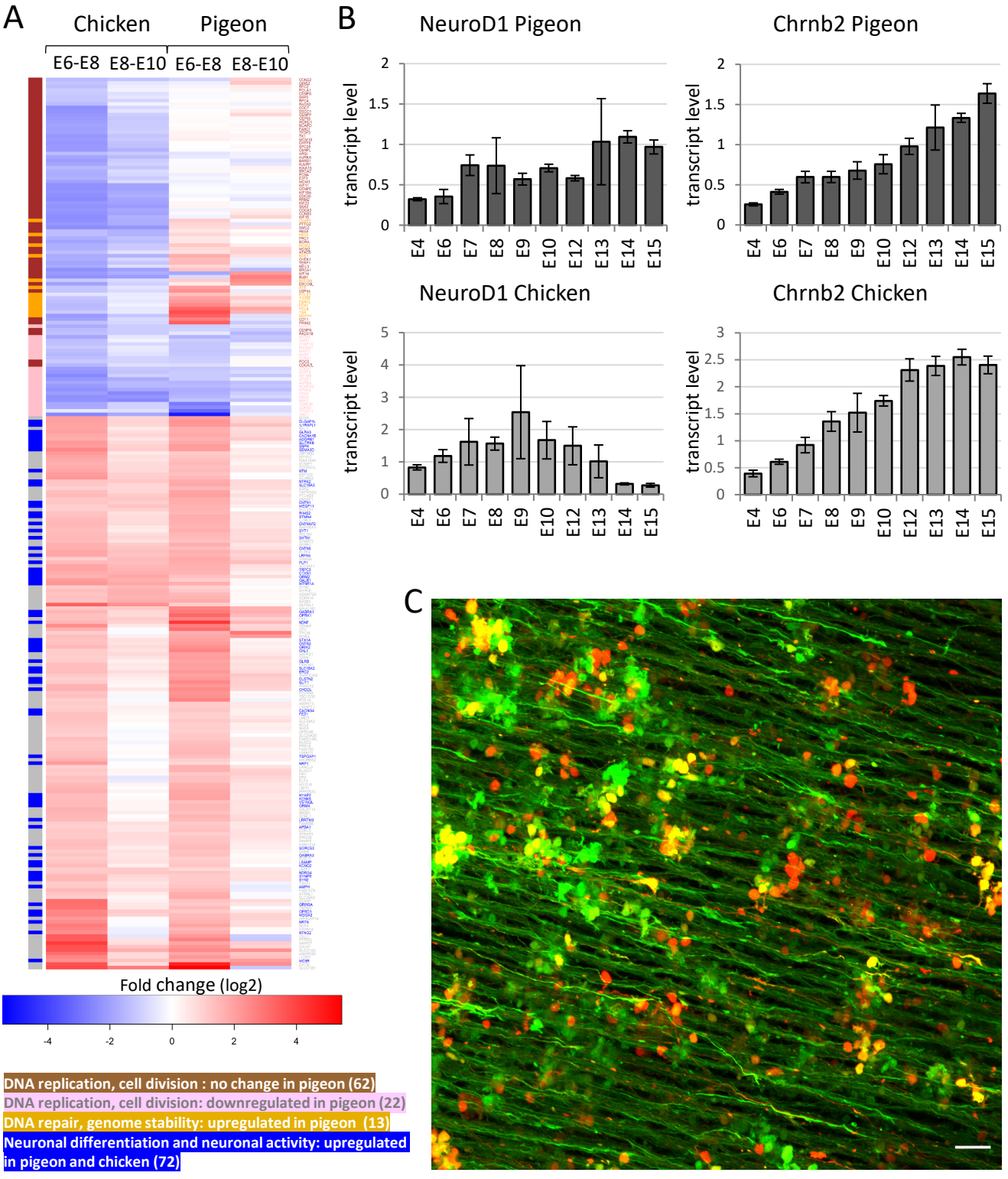
A
Chicken
Pigeon
E6-E8
E8-E10
E6-E8
E8-E10
Fold change (log2)
-4
-2
0
2
4
B
NeuroD1 Pigeon
Chrnb2 Pigeon
NeuroD1 Chicken
Chrnb2 Chicken
transcript level
E4
E6
E7
E8
E9
E10
E12
E13
E14
E15
C
DNA replication, cell division : no change in pigeon (62)
DNA replication, cell division: downregulated in pigeon (22)
DNA repair, genome stability: upregulated in pigeon (13)
Neuronal differentiation and neuronal activity: upregulated in pigeon and chicken (72)

**Figure 7 - Transcriptomic analysis of the pigeon and chicken OT.** (A, upper panel) Heat maps generated from RNA-Seq data showing clustered genes regulated during the two periods between E6 and E10. (A, lower panel) In chicken, 97 genes known to regulate DNA replication and cell division are downregulated between E6 and E10. In pigeon, 62 orthologs (gene symbol in brown) show no significant change in expression, 22 orthologs (gene symbol in pink) are downregulated, 13 orthologs (gene symbol in orange) are upregulated between E6 and E10. Out of the 166 genes upregulated in both pigeon and chicken during the period between E6 and E8, 72 genes (gene symbol in blue) are known to be involved in neuron differentiation and neuron activity. 94 genes (gene symbol in grey) have not been submitted for gene ontology analysis. (B) Accumulation of NeuroD1 and Chrnb2 transcripts measured by RT-qPCR analysis. At each developmental stage, data are from three biological replicates and presented as mean ± s.d. (C) Axons of neurons residing in the VZ. The pigeon OT was co-electroporated in ovo with Hes5.3-GFP and CMV-RFP reporter plasmids at E4. Fluorescent axons and somas were visualized by confocal microscopy at E7. The image plane is normal to the apico-basal axis and situated at the level where radial glial fascicles abut the VZ. Parallel bundles of axons are at intervals corresponding to the distance between the radial fascicles (5-10 µm; Figure 5B). Few GFP- and/or RFP-labelled cell bodies are scattered between axons. Scale bar: 20 µm.

### *10. Unlocking cell migration*

In pigeon, few cells had moved in the interspaces between radial glia fascicles until E9, while at E10, cells migrated through the glial scaffold (layer i) for establishing the outer layers (Figure 8D), a pattern resembling the one in chicken at E7 (Figure 5A). Cell migration out of the VZ coincided with tissue folding that led to the deepening of the median tectal groove and the separation of the two lobes three days later than in chicken (Figure 8A). About half of the cells have already left the VZ at E10 and the proportion of cells in the layers i and ii were the same in the dorsomedial and ventrolateral sectors (Figure 8B). This is different from the situation in chicken where the retarded dorsomedial sector is ~2 days behind the development of the ventrolateral sector (LaVail and Cowan, 1971b).

### *11. Cell migration in pigeon and chicken are regulated by different sets of genes*

In the chicken OT, neuronal precursors migrate and establish layers between E6 and E8 (Gray and Sanes, 1991; LaVail and Cowan, 1971b), whereas, in pigeon, neurons get stuck in the VZ up to E9. We asked how this spectacular interspecies difference was related to changes in gene regulation. Evsyukova et al. (2013) have compiled a comprehensive list of 165 genes that regulate cortical neuronal migration in mammals. Our transcriptomic data show that 46 genes from this list were up or downregulated in chicken between E6 and E8, whereas their expression did not significantly vary in pigeon. During the same period, 17 genes were up or downregulated in both species (Figure 9A). These two sets of genes encode receptors, secreted molecules, substrate- or membrane-bound molecules or transcription factors that might be involved in cell migration and/or axon growth and guidance. In pigeon, neurons extended axons while their somas still resided in the VZ (Figure 7C), suggesting that the 17 genes differentially expressed in both pigeon and chicken (e.g., SLIT1, MAP2, Figure 9A) are likely to be involved in axon growth. One striking feature of our data is that none of the 46 genes differentially expressed in chicken between E6 and E8 were differentially expressed in pigeon between E8 and E10 - i.e., during the period when neurons migrate out of the VZ (Figures 8, 9A). The difference in status of migrating cells - i.e., neural precursors in chicken vs. neurons in pigeon - could be one of the reason why different gene regulatory networks are involved in cell migration in each of the two species. In the developing mouse telencephalon, Nkx2-1 represses the expression of Neuropilin-2 (Nrp2) and the downregulation of Nkx2-1 is a necessary event for the migration of interneurons to the cortex (Nobrega-Pereira et al., 2008). In the same way, Nrp1 and Nrp2 were upregulated while Nkx2-1 was strongly downregulated in the chicken OT (+2.11 and +2.55 in log2 for Nrp1 and Nrp2; -7.03 in log2 for Nkx2-1; Figure 9A). However, these genes were not differentially expressed in pigeon. The upregulation of the β1 integrin, ITGB1, and of the ligands and activators of integrin, CXCL12, in pigeon are clues pointing to neuron migration dependent on the integrin signaling pathway

(Figure 9A, see also Galileo et al. (1992)). The upregulation of the GDNF family receptor alpha GFRA1 and the downregulation of the adhesion molecule NCAM1 in pigeon between E8 and E10 (Figure 9A) are consistent with this idea. In this context, it is worth mentioning that by impeding the function of NCAM, GFRA1 promotes the migration of Purkinje cells in the developing mouse cerebellum (Sergaki and Ibanez, 2017).

We have been intrigued to find that genes encoding extracellular matrix structural and non-structural constituents [Decorin (DCN), Lumican (LUM), Cartilage acidic protein 1 (CRTAC1) Osteoglycin (OGN), Otolin (OTOL1)], components mediating cell-matrix interactions [Laminin (LAMA1)] and tight junctions' proteins [claudins (CLDN1)] were strongly downregulated at the onset of cell migration in chicken, while their expression did not vary in pigeon, except for OTOL1 and CRTAC1 which were upregulated (Figure 9B). DCN, LUM, CRTAC1, OGN, CLDN1 have the capacity to impede cell movement and could, for some of them, inhibit metastasis (Appunni et al., 2019; Deckx et al., 2016; Hagen, 2017; Karamanou et al., 2021; Yang et al., 2021). The idea that these molecules may contribute, in different ways, to pose physical barriers that prevent cells to migrate out of the VZ is strengthened by the fact that genes encoding the matrix metalloproteases MMP1 and MMP27 were strongly upregulated in chicken, whereas they were upregulated weakly or not at all in pigeon (Figure 9B). The spectacular cross-species differences in the patterns of expression of genes that regulate cell migration could be one crucial feature of the divergence in OT development between pigeon and chicken and, more broadly, between diurnal Neoaves and Galloanserae.

Figure 8

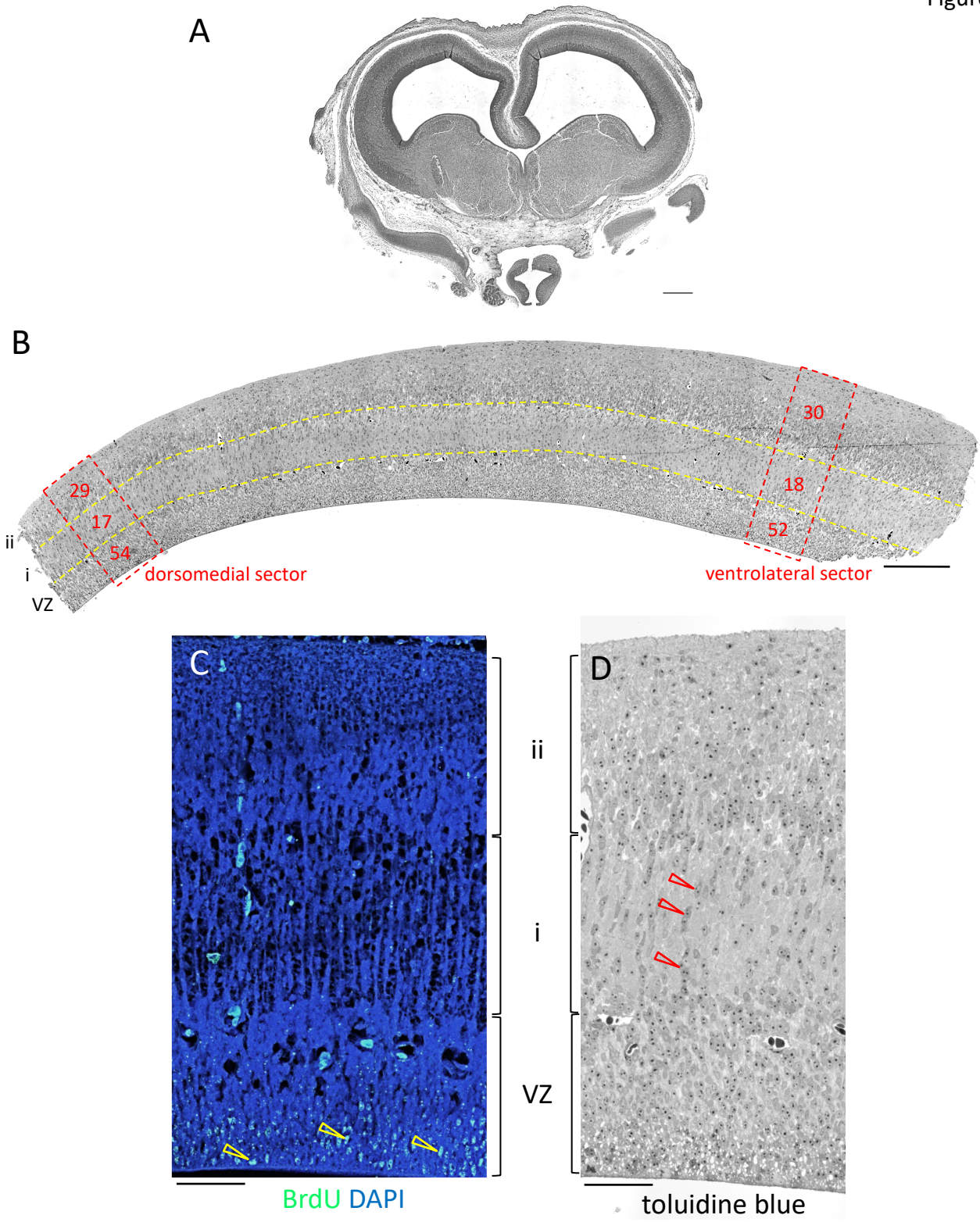
A
B
29
17
54
30
18
52
ii
i
VZ
dorsomedial sector
ventrolateral sector
C
D
ii
i
VZ
BrdU DAPI
toluidine blue

**Figure 8 - Unlocking cell migration in pigeon.** (A) Low magnification picture of a frontal section through the pigeon OT at E10. The separation of the two lobes is underway. (B) Semi-thin section along the dorsoventral axis of the OT at E10. The values in the frames correspond to the proportion of cells (%) in the three layers (VZ, i, ii) delimited by the dashed lines. (C) BrdU was injected in ovo at E8. The OT was isolated at E10 and sections were processed for immunohistochemistry and counterstained with DAPI. Labelled cells (some of them are indicated by yellow arrowheads) are localized on the apical side of the VZ. (D) Semi-thin section of the central OT at E10. Numerous cells migrate between meshwork of radial fibers in the layer i (some of them are indicated by red arrowheads). Scale bars: 500 µm (A), 200 µm (B), 50 µm (C, D).

**Figure 9 - Genes regulating cell migration are differentially expressed in pigeon and chicken OTs.** (A, B) Bar graph generated from RNA-Seq data. Positive or negative fold changes in log2 are presented (on y-axis). (A) The graph shows a selection of 83 genes known to regulate cortical neuronal migration and axon growth. 46 genes are up or downregulated (>1 or <-1 in log2) in chicken between E6 and E8. None of them are differentially expressed in pigeon between E6 and E8 or between E8 and E10. 17 genes were up- or downregulated in both species between E6 and E8. (B) The graph shows the regulation of genes encoding extracellular matrix components or matrix metalloproteinases.

Figure 9

A

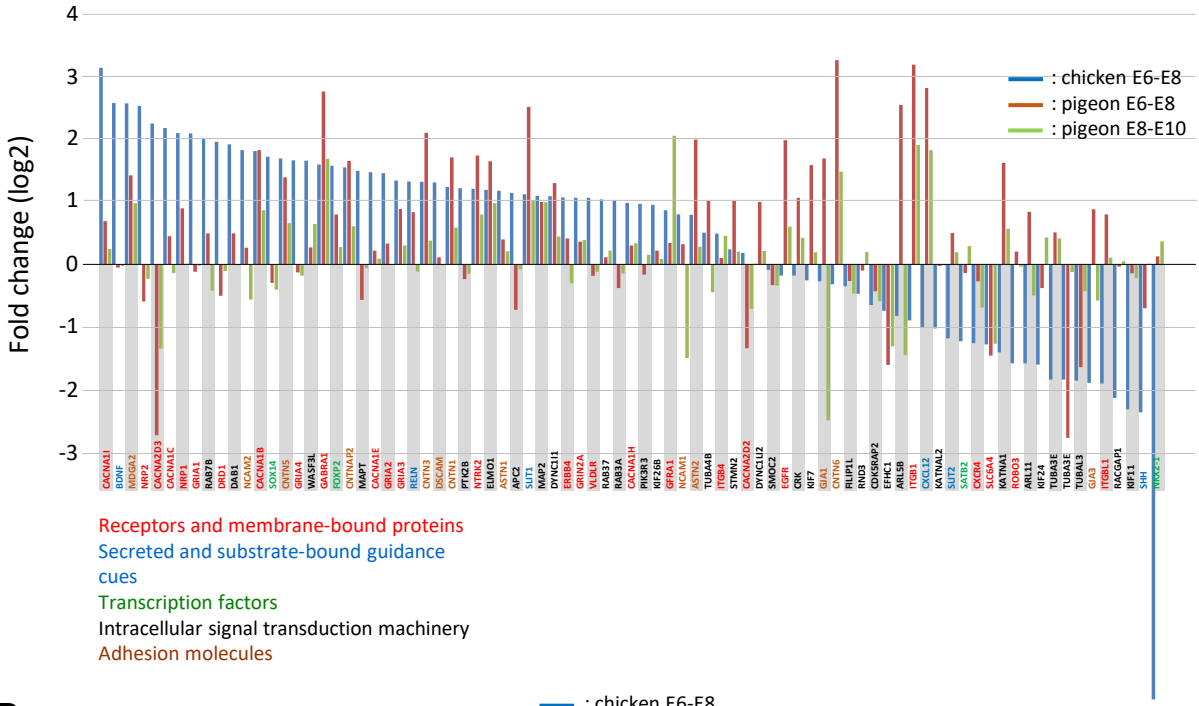


Receptors and membrane-bound proteins
Secreted and substrate-bound guidance cues
Transcription factors
Intracellular signal transduction machinery
Adhesion molecules

B

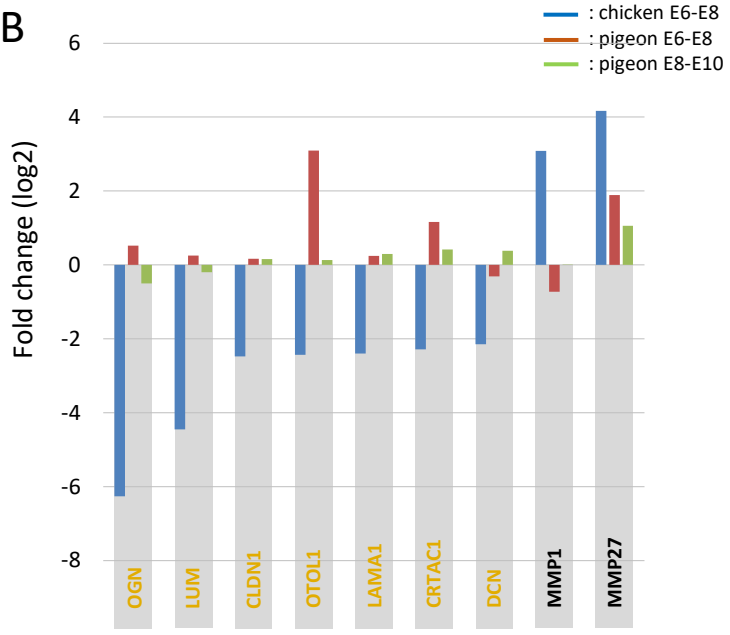


Extracellular matrix components
Proteases

### *12. Fate and positioning of cells produced by the late pool of progenitors*

Cross-species differences in the timing and regulation of cell migration raise questions in the context of the lamination of the optic tectum and, in particular, of its 'inside-out' type of developmental gradient. In this perspective, we wanted to determine the fate and the positioning of cells produced by the late pool of progenitors in pigeon. BrdU was injected in ovo at E8 and tissue sections were probed at E10 or E12 (Figures 8C, 10A, B). At E12, all labelled cells have migrated in the most superficial layers of the tectum, indicating that progenitors dividing beyond E8 were in their vast majority committed to produce cells of the SGFS. At E10, BrdU-labelled cells still resided in the VZ (Figure 8C) indicating that, in pigeon, like in chicken (LaVail and Cowan, 1971b), cells of the SGFS migrated according to an 'inside-out' developmental gradient. The fact that BrdU-labelled cells were uniformly distributed along the rostro-caudal axis at E12 (Figure 10A), suggests a temporal coincidence of the production of SGFS neurons all over the OT. The absence of identifiable gradients of cell genesis comparable to that observed in chicken (LaVail and Cowan, 1971b) is reminiscent of the much less marked central-to-peripheral gradient in the emergence of RGCs in pigeon than in chicken retina (Rodrigues et al., 2016). Taken together, our data show that the proliferation of a late pool of progenitor cells and the radial expansion of ontogenetic columns between E7 and E9 (Figures 5A, S4) have the effect of increasing the number and density of SGFS neurons who, for the most part, could be involved in retino-tectal connections. Although RGCs are the first neurons born in the retina and SGFS neurons are the last-born, genesis of the two cell types peaks around the same time – i.e., E6 in chick, E9 in pigeon (Figure 10D). This coincidence is not contingent upon axon connection that occurs at later stages of development (Rodrigues et al., 2016).

Figure 10

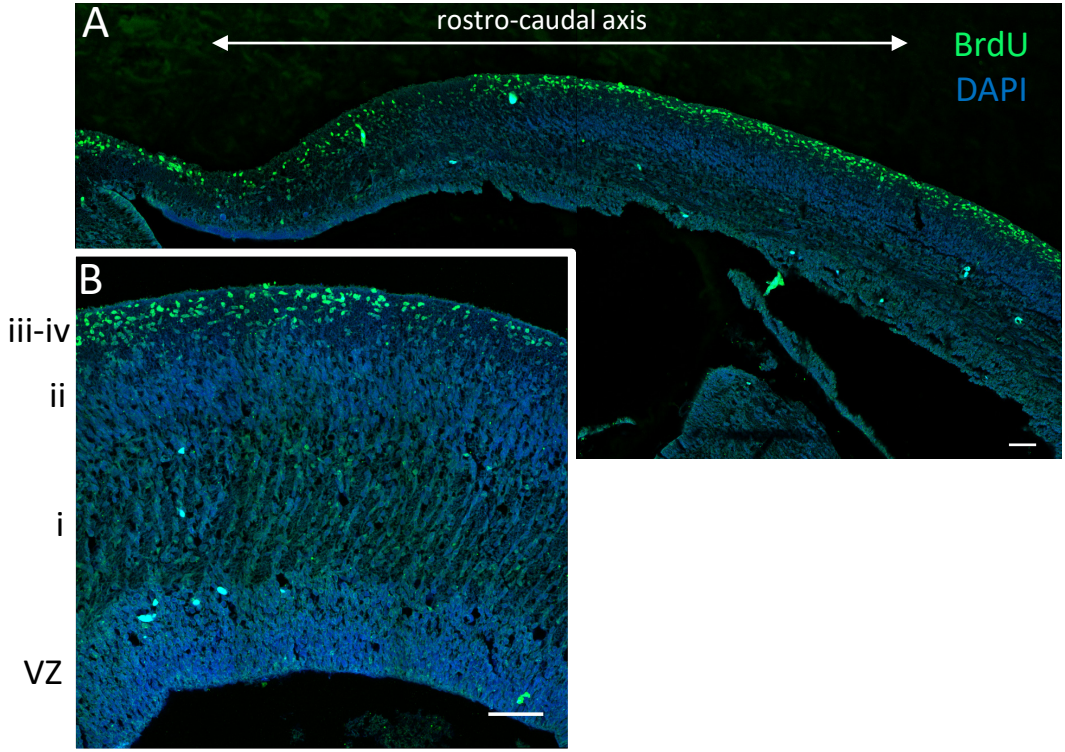
A
rostro-caudal axis
BrdU
DAPI
B
iii-iv
ii
i
VZ

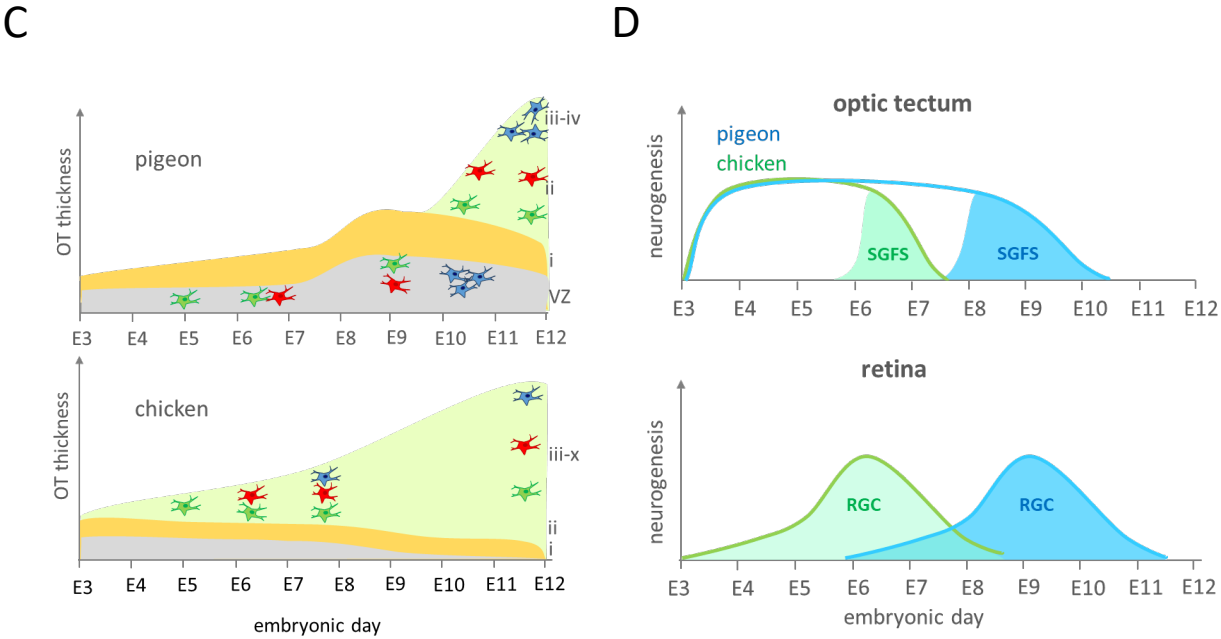
C
pigeon
OT thickness
iii-iv
ii
i
VZ
E3 E4 E5 E6 E7 E8 E9 E10 E11 E12
chicken
OT thickness
iii-x
ii
i
E3 E4 E5 E6 E7 E8 E9 E10 E11 E12
embryonic day
D
optic tectum
pigeon
chicken
neurogenesis
SGFS
SGFS
E3 E4 E5 E6 E7 E8 E9 E10 E11 E12
retina
neurogenesis
RGC
RGC
E3 E4 E5 E6 E7 E8 E9 E10 E11 E12
embryonic day

**Figure 10 - Fate and positioning of cells produced by the late pool of progenitors in pigeon.** (A, B) BrdU was injected in ovo at E8. The OT was isolated at E12. A section along the rostro caudal axis (A) or a cross section (B) were processed for immunohistochemistry and counterstained with DAPI. All labelled cells are localized in the most superficial layers of the SGFS (layers iii and iv). (C) A diagram that outlines OT development in pigeon and chicken. In chicken, the newborn neuronal precursors leave the VZ, migrate through the glial fibers (layer i) to occupy their position in the outer layers (layers ii-x) according to an 'inside-out' developmental gradient, meaning that later-generated neurons (e.g., "blue" neuron) settle in progressively more superficial tectal layers. In pigeon, neurons do not leave the VZ until SGFS neurons arising from a late pool of progenitors have been generated. The ~3-fold increase of neuron density in the pigeon SGFS compared to chicken results from: (1) postponed cell migration, (2) prolonged cell proliferation, (3) hindered lateral expansion of the OT. (D) A diagram that outlines neurogenesis in the OT and retina. SGFS neurons are the last-born in the OT, whereas RGCs are the first neurons born in the retina. The production of SGFS neurons and RGCs are delayed by ~3 days in pigeon. The genesis of the two cell types coincides in each of the two species. Scale bars: 50 µm (A, B).

## DISCUSSION

Our cross-species comparisons revealed that cell density in the SGFS of the OT was two to four times higher in birds with one or two foveae compared to birds with no fovea. Although this increase of cell density may look quite modest, we show that it requires spectacular changes in tissue morphogenesis and gene expression during embryogenesis. We can reasonably assume that increased densities of RGCs in the retina and of SGFS neurons in the OT of Neoaves with one or two foveae contribute to enhance their spatial and temporal visual acuity. A popular belief is that bird's eyes send a much more processed image to the brain than our eyes send to our brain, which imply that there is less brain processing in birds than in primates (e.g., Schwab et al., 2012). However, our results are somewhat at odds with this idea as they would rather suggest that foveal vision does require an increase in the processing capacity of the brain. The emergence of the fovea in modern birds can be seen as an evolutionary breakthrough that had a decisive influence on flight, feeding habits and lifestyle. Birds became lightweight by reducing their size and evolving thin and hollow bones. The ease with which they fly and catch prey through cluttered airspaces would not have been possible without this major adaptation of their visual system. Setting up structures such as the fovea required major developmental and behavioral changes for postponing the completion of retina and brain maturation well beyond hatching, hence requiring prolonged parental care. In a wider perspective, altriciality that has developed in Neoaves ancestors may have relaxed constraints on the duration of ontogenesis, a precondition for expansion of the brain as suggested by Charvet and Striedter (2011).

The developing tectum shares features with mammalian cerebral cortex and has been viewed for a long time as a model of corticogenesis (e.g., Gray and Sanes, 1991; Hamdi and Whitteridge, 1954; LaVail and Cowan, 1971a). Gray and Sanes (1991) provided a thorough clonal analysis highlighting how migratory pathways influence cell fate determination in the developing chicken OT. They found that *"cells descended from a single progenitor begin to migrate together, but that subgroups then diverge to form three distinct streams that follow distinct guides and differentiate into distinct sets of cell types"*. Our data indicate that there is no relationship between cell migration and cell fate determination in the pigeon. One reason that could justify a drastic shift in development strategy is the necessity for pigeons to increase neuron density to levels that could not be achieved in chickens. Owing to changes in development pattern, the pigeon can increase twice the absolute cell density in its tectal lobes, thereby reaching a total number of cells equivalent to that of the chicken (~$40x10^6$ cells), yet in a tissue volume twice smaller. Cell numbers and tissue sizes increase in similar proportions in both species up to E7. Then, each species follows its own development trajectory. In chicken, tectal cells stop to proliferate and newborn neural precursors migrate to establish the

outer layers. In pigeon, neurons differentiate while they are stuck in the VZ until the expansion of a pool of late progenitors does complete. This prolonged cell proliferation leads to a thickening of the VZ along its radial axis rather than to its tangential expansion. With this innovative change in tissue morphogenesis, the number of cells in radial columns almost doubles, thereby setting the stage for an increase of cell densities in the outer layers once SGFS neurons did migrate (Figure 10C). We identified the earliest divergence in tissue morphogenesis when the first neurons were moving through the outer radial fibers in chicken, whereas, in pigeon, they stayed in the VZ. This observation was corroborated with the finding that a set of genes known to be involved in the regulation of cell migration were differentially expressed in chicken but not in pigeon. The uncoupling between cell differentiation and cell migration is unprecedented and raises several questions, in particular, how the VZ in pigeon provides conditions conductive to neuron differentiation, axon growth and cell positioning.

The retinas of less than 1% of the ~10’500 bird species have been studied so far. The general trend is, however, that densities of RGCs and cones are higher in diurnal Neoaves than in Galloanserae. Higher RGC density in pigeon in comparison with chicken results from delayed neurogenesis with respect to eye growth (Rodrigues et al., 2016). While about half of retinal cells exit the cell cycle and differentiate at early embryonic stages in chicken, cells stay in the pool of proliferating progenitors for about three more days in pigeon. This strategy has the disadvantage of postponing retina development beyond hatching. In precocial Galloanserae, the need for a functional visual system at the time of hatching requires the production of RGCs at early stages, thereby de facto limiting their number. In pigeon, high level of retinoic acid and robust mitochondrial activity contribute to maintain retinal progenitors in proliferation, thereby prolonging their uncommitted status (Brodier et al., 2021; Cherix et al., 2020; Rodrigues et al., 2016). At the end of neurogenesis, the density of newborn RGCs is about three times higher in pigeon than in chicken. In pigeon, the subsequent stretching of the retinal tissue leads to a decrease in RGC density, except for a central region identified as the incipient fovea. It appears that the prolonged cell proliferation and hindered tangential tissue growth are the basic elements at work for increasing neuron densities in the fovea and in the foveal confluence of the OT.

Despite its importance, little is known about foveal vision in birds. The fact that cell densities in the MT3 sector are consistently higher in birds with a central fovea suggests that this region of the tectum encompasses the central foveal confluence. In pigeon, Clarke and Whitteridge (1976) localized the fovea projection by observing the visual fields of points obtained with a grid of electrode. An area with the greatest magnification factor (length along tectal surface per degree of visual field) was taken as the projection area of the fovea. While the localization of this area roughly coincides with our MT3 sector, future studies should define its exact

position, size and shape. In the human fovea, the one cone to one RGC relationship in the so-called midget pathways is presumed to be the substrate for sharp vision. However, the human fovea is not well adapted to process rapidly changing visual signals - i.e., movement perception. This low temporal acuity is what makes us see motion rather than a sequence of individual images in movies or flip books. Behavioral experiments to estimate temporal visual acuity have shown that birds can resolve alternating light-dark cycles at up to 145 Hz, which is >50 Hz over the highest frequency shown in human and in any other vertebrate (Bostrom et al., 2016). Does the need to track moving objects at high-speed explain a fundamental change in the way the fovea is built and operates in birds? The three species of fast flyers catching insects on the wing (C. House-Martin, Barn Swallow, C. Swift) have fully developed central and/or peripheral foveae and the highest neuron densities in the SGFS among the studied birds. This stands in stark contrast, however, to the fact that the cone and RGC densities in the peripheral fovea of swallows and swifts are in several instances lower than in foveate birds with no peripheral fovea. The peripheral retina of the E. Sparrowhawk displays the highest RGC density among all species, yet cell density in the SGFS is lower than in species with a peripheral fovea. This somewhat paradoxical situation could indicate that for RGCs transmitting foveal visual signals, the number of tectal neurons they connect is higher than for extra-foveal RGCs. In the hawk's peripheral retinas, the ratios of RGCs to cones are equal or close to 1, suggesting the predominance of extra-foveal circuits resembling the midget pathways of primates. On the other hand, in ten out of the twelve foveae surveyed in this study, the ratios of RGCs to cones are below 0.6, suggesting that non-midget ganglion cells that receive (indirect) input from multiple cones may form alternative circuits in the bird fovea. Presence of foveal circuits with wider range of sensitivity to rapid variations in light input than in primates (Sinha et al., 2017) might provide the fovea with both high temporal and high spatial acuity, a decisive factor for birds to perceive motion in high resolution.

MATERIALS AND METHODS

***Animals***

Eyes and brains were collected from wild birds with unrecoverable injuries who have been euthanized at the rehabilitation center La Vaux-Lierre (http://www.vaux-lierre.ch). Fertilized pigeon eggs were supplied by Philippe Delaunay and François Jardin (https://www.pigeonneau-normand.com/). Chicken eggs were supplied by the animal resources centre of the University of Geneva (http://www.medecine.unige.ch/zootechnie). Adult domestic and homing pigeons were provided by François Jardin (https://www.pigeonneau-normand.com/). Adult quail and adult chicken were provided, respectively, by Marc Plancherel (https://www.oeuf-de-caille.com/) and the Fournier company (http://www.etsfournier.ch/). Birds were euthanized and tissues were collected in accordance with Federal Swiss veterinary regulations.

***Standardized tissue isolation and processing***

There is a rapid decay of retinal and brain tissues in euthanized adult birds. The eyes and the brain were dissected and collected in DPBS (ThermoFisher) less than 20 min after death. The retinas and the OT were isolated and prefixed in 3.7% formaldehyde, 1% glutaraldehyde, 0.1 M Sodium phosphate monobasic, 0.07 M NaOH in distilled water at 4°C for 30 min. This 1$^{st}$ fixation increased tissue stiffness and helped for precise cuts. Tissue cubes of 2 to 4 millimeters side encompassing the different sectors of the retinas and OT were incubated at 4°C for a 2$^{nd}$ period of fixation that lasted until embedding in the epoxy resin. The tissue samples were washed with 0.1 M ice cold sodium cacodylate before incubation 10 min in 0.8% $K_3Fe(CN)_6$ in 0.1 M sodium cacodylate and fixation in 1% osmiumtetroxide, 0.8% $K_3Fe(CN)_6$ in 0.1 M sodium cacodylate pH 7.4 for 90 min. They were washed with sodium cacodylate and water, stained 2 hours with 1% uranyl acetate, dehydrated in ethanol baths and incubated in propylene oxide 100% for 45 min, followed by propylene oxide/epon 1:1 incubation overnight. Tissue cubes were embedded in the proper orientation in epoxy resin consisting of 48% Agar 100, 18% DDSA, 31% MNA and 3% BDMA (agar scientific). Semi-thin (1 µm thick) sections were produced using a Leica UCT ultra-microtome and were mounted on glass slides (SuperFrost/plus, Assistant).

***Morphometric measurements***

*Computing cell number and cell area on tissue sections*

Plastic sections 1 µm thick from embryonic and adult OT and adult retina mounted on glass slide were stained by incubation 1-2 minutes in 1% toluidine blue (Sigma Aldrich), 1% sodium borate in distilled water. Coverslips were sealed with xylene-free EUKITT® neo (O. Kindler

ORSAtec). Images were acquired with a Zeiss LSM 800 microscope. With the help of tile regions, we acquired areas with dimensions that exceeded the size of an individual image field. Tiles were arranged in the form of a grid with a Zeiss image-processing software. To compute the cell number in embryonic OT and adult retina, each cell body was manually annotated by surrounding it with a closed line using an image analysis software (ImageJ/Fiji). Cells were counted in vertical frames partitioning the whole tectal or retinal section, each one of them having a width of 25-50 µm. To compute the areas of cell bodies in the retina GCL, the pixels inside the closed curve were counted using a geometry processing tool (Python library Shapely). The number of pixels was then converted to the area in $\mu m^2$. After a test phase, we found that the counting of cell nuclei in adult OTs was more reliable when it was conducted under the microscope. The 36 resin blocks of tectal tissues (12 species and 3 sectors per species) were cut in a plane perpendicular to the tissue layers at a distance from the surface of the block that varied between 200 and 300 µm depending on the penetration depth of the fixative solution and the preservation of the tissue. Sets of four 1 µm thick sections were collected every ~50 µm, mounted onto a glass slide (SuperFrost/plus, ThermoScientific), stained with toluidine blue, washed and air dried. From a total of 16 to 24 sections per block, 8 sections of the highest histological quality were selected. Nuclei with visible nucleoli were counted using a Nikon Diaphot inverted microscope equipped with a Nikon Fluor 40/1.30 oil objective and an eyepiece reticle (50 µm x 60 µm at the selected magnification). The counting frame was displaced across the whole area of the section encompassing the SGFS. The scanned areas varied from sectors to sectors and from specimens to specimens. On a total of 8 sections, nuclei were counted in 24 to 211 frames (referenced on the Figure 1B, x-axis). The counting of 4575 frames was carried out over a period of several months. To minimize bias in the counting procedure, tectal nuclei were counted and sometimes recounted in different specimens and sectors according to a mixed sample list. For instance, the nuclei on one section of the MT1 sector of the species x and the nuclei on one section of the MT2 sector of the species y were counted the same day, while the nuclei on another section of the MT1 sector of the species x and the nuclei on one section of the MT3 sector of the species z were counted another day.

*Isotropic suspensions of nuclei*

One optic tectum (2 lobes) was dissected and washed in ice-cold PBS. A Dounce glass homogenizer was manually operated for shearing cells in 100 µl of lysis buffer consisting of 10 mM Tris-Cl, pH 7.5, 10 mM NaCl, 3 mM $MgCl_2$ and 0.5% Triton X-100. Only perfectly homogenous nucleus suspensions were selected for counting. Nuclei were counted with a Neubauer chamber by phase-contrast microscopy.

*3D reconstruction of the OT*

The OT was dissected, fixed in 4% paraformaldehyde and paraffin-embedded. Properly oriented OT was cut in a plane perpendicular to the rostro-caudal axis. Every section of the ribbon of serial 10 µm thick sections was mounted on glass slides. Sections were deparaffinized and stained. Low-magnification picture of all sections were taken. To compute the surface area, each section was manually annotated by surrounding it with a closed line using an image analysis software (ImageJ/Fiji). The total volume of a dehydrated optic tectum ($\mu m^3$) was equal to the sum of the volume of each section (i.e., surface area [$\mu m^2$] x 10 µm).

***Reporter plasmid***

The Hes5.3-GFP plasmid derive from pEGFP-C1 plasmid (Clontech). The fragment bounded by the AseI and NheI restriction sites was deleted from pEGFP-C1 and the upstream sequences of Hes5.3 (1960 bp in length, Chiodini et al. (2013)) were subcloned in the proper orientation at appropriate sites in the vector.

**In Ovo Electroporation**

One hour prior to the electroporation, the eggs were rotated for half a turn so that the embryos that were sitting on the top were now at the bottom of the egg. Egg candling with a smartphone's flashlight 1 hour later allowed to select eggs with the embryo back on the top. This test indicated that the membranes were not sticking to the shell. A piece of transparent tape was placed at the embryo position and a small hole was pierced with a forceps at the position of the air chamber. This allowed the embryo to sink before cutting the shell. A solution of DNA plasmid (1 µg/µl) and fast green dye (0.025%) in PBS was injected in the ventricle of the OT with a glass capillary mounted on a Hamilton syringe. The tweezertrodes electrodes (BTX) connected to a BTX generator were positioned on both sides of the embryonic head. We most often use the following settings: five 12.5 V/cm pulses of 50 milliseconds duration with 1 second pause between each. The window was closed using tape and the egg was incubated until reaching the desired stage.

**Confocal imaging of the optic tectum**

Electroporated OTs were fixed with 4% paraformaldehyde for 20 min and were mounted on concave glass slides. Coverslips were sealed after addition of DABCO with 50% glycerol (Sigma-Aldrich) in DPBS. Images were acquired with a Zeiss AXIO Imager Z1m microscope.

**BrdU labelling**

*In ovo*

Pigeon embryos received a single dose of 5-Bromo-2′-deoxy-Uridine (100 µl of PBS containing 10 mM BrdU) into the chorioallantois, through a window made in the shell the date of injection. The window was sealed with transparent tape, and the egg returned to the incubator.

*Ex vivo*

The optic tectum explants were incubated in 35 µM BrdU, in Dulbecco's Modified Eagle Medium (DMEM), 10% fetal bovine serum (FBS) for 1 or 19 hours. The explants incubated for 1 hour in BrdU were transferred in DMEM, 10% FBS for 1 hour, rinsed in PBS, fixed in 4% paraformaldehyde and embedded in paraffin. Tectal cells of the explants incubated for 19 hours in BrdU and were dissociated in 0.1% trypsin in Hanks' Balanced Salt Solution (HBSS) without $Ca^{++}$ and $Mg^{++}$. 50 µl of DNase and 500 µl of FBS were added 5 and 15 min later. The cell suspension was centrifuged and the pellet was resuspended in DMEM. Cells were counted with a Neubauer chamber and $10^5$ cells in a 100 µl drop were deposited on a polyornithine-coated plastic chamber slide (Lab-Tek). Slides were incubated at 37°C for 1 hour to allow cell attachment, fixed in 4% paraformaldehyde for 20 min, rinsed in PBS and air dried.

*Immunostaining*

Deparaffined sections (8 µm thick) or dissociated cells were rehydrated, rinsed in PBS and incubated 10 min (dissociated cells) or 15 min (tissue sections) in 4N HCl. After neutralization in PBS, 0.5% BSA, 0.1% Triton X-100, cells and sections were processed for BrdU immunodetection following the manufacturer’s recommendations (5-Bromo-2′-deoxy-uridine Labelling and Detection Kit I, Roche). The slides were mounted for fluorescent microscopy in ProLong® Diamond Antifade Mountant with DAPI (Life Technologies).

**RT-qPCR**

RNA from whole OT was extracted using TRIzol reagent (ThermoFisher) according to product manual in triplicate. Primers were designed using NCBI primer blast and Primer 3 websites. Primers were ordered from Microsynth. Primers were tested using RNA from total retina extracted with TRIzol. RNA quantification was done with spectrophotometer and Qubit 2.0 (ThermoFisher) and RNA quality was checked using BioAnalyzer 2100 (Agilent). RT was performed using Takara PrimeScript reverse transcriptase prior to qPCR. In samples with delta-Ct values > 0.5 across the three technical replicates, the most extreme value was removed. Quantities were calculated as 2^(Ctmin-CT). The Average-Quantity was calculated for each sample. GeNorm (Vandesompele et al., 2002) was used to determine the best normalization genes. A normalization factor was calculated as Normalization-Factor ¼

Geometric Mean [Average-Quantity of Normalization Genes] and was used to calculate the normalized quantity: Normalized-Quantity ¼ Average-Quantity/Normalization-Factor. The fold change was calculated as: Fold-Change ¼ Mean [Experiment condition]/Mean [Baseline condition]. P-values were calculated using a Welch t-test to compare baseline and experiment samples (in log 2 scale). RT-qPCR were performed using the primers listed in Table S4. All specific primers for chicken and pigeon listed in Table S4 were tested for efficiency.

**RNA-Seq**

*Tissue collection*

We collected 5 biological replicates for each of the three developmental stages (E6, E8 and E10) of pigeon and chicken OT (30 samples). Total RNA was extracted and quantified with a Qubit (fluorimeter from Life Technologies) and RNA integrity assessed with a Bioanalyzer (Agilent Technologies).

*RNA sequencing*

A total of 30 RNA sequencing libraries was generated. Libraries were prepared with TruSeq Stranded RNA Library Prep Kit (Illumina) and sequenced on multiple lanes of an Illumina HiSeq2500 platform, generating paired-end 100-cycle reads for each sample. The quality of sequence was assessed by FastQC (version v0.11.4, available online at: http://www.bioinformatics.babraham.ac.uk/projects/fastqc/ (Andrews, 2010). Purity-filtered reads were adapters- and quality- trimmed with Cutadapt (v1.8) (Martin, 2011). Reads matching to ribosomal RNA sequences were removed with fastq_screen (v. 0.9.3). Remaining reads were further filtered for low complexity with reaper (v. 15-065) (Davis et al., 2013).

*Chicken gene annotation*

Gallus Gallus reads were then aligned against Gallus_gallus-5.0.92 genome release using STAR (v.2.5.2b) (Dobin et al., 2013). The number of read counts per gene locus was summarized with htseq-count (v0.6.1) (Anders et al., 2015). Quality of the RNA-seq data alignment was assessed using RSeQC (v. 2.3.7) (Wang et al., 2012).

*Pigeon gene annotation*

Pigeon genome (Cliv_1.0 assembly from 2014-02-18) was obtained from the (GIGA)n database (gigadb.org). Since Columba livia is not a model organism we annotated the genes by comparing Columba livia gene sequences to Gallus Gallus genes. We realized a protein sequence mapping between pigeon and chicken using blast by keeping the maximum score hit.

*Differential Expression Analysis*

To assess differential expression between embryonic development stages of the pigeon and chicken, we compared the foldchange of significantly differentially expressed genes between E6 and E8 and between E8 and E10. Data analysis has been performed with the R Bioconductor package DESeq2 (version 1.14.1) (Love et al., 2014). Differentially expressed genes (DEGs) were identified at the Benjamini-Hochberg (BH) adjusted P < 0.05 level, using Wald test. The function of avian genes is poorly annotated. Potential functions of differentially expressed genes were manually extracted from published data about the function of chicken, human and mouse orthologs.

**Statistical analysis of morphometric data**

All computations and graphics were done using Python v3.9.2 (libraries: Matplotlib v3.4.2., Numpy v1.20.2, Scipy v1.6.3, Shapely v1.8a3). The Kernel Density Estimation (KDE) used for drawing the violin plots (Figures 1B, S2B) consists in extracting an empirical probability density function from the data (i.e., a non-negative function whose area under the curve equals one). Given a set of $n$ data points $x_1, \dots, x_n$, the density estimate at a point $x$ is obtained as

$$f_K(x) = \sum_{i=1}^{n} K(x - x_i\,, h)$$

where $K(x, h)$ is a positive function controlled by a bandwidth parameter $h > 0$. One can think of the kernel $K(x, h)$ as a smoothing sliding window of width $h$ which can have different shapes. The shape of the kernel reflects the weight of a data point $x_i$ located at a given distance of the estimated point $x$. We used a kernel with a gaussian shape :

$$K(x, h) \propto \; exp\left(-\frac{x^2}{2h^2}\right).$$

The kernel is appropriately normalized so that the area under the curve $f_K$ equals one. The bandwidth parameter $h$ was set according to Scott's Rule :

$$h = \frac{\sigma^2}{\sqrt[5]{n}}$$

where $\sigma$ is the computed standard deviation of the data.

The red curve $g$ (Figure S3) is obtained by smoothing the binned values $x_1, \dots, x_n$ with a gaussian kernel

$$g(x) = \sum_{i=1}^{n} x_i \cdot K(x - x_i\,, h)$$

where $K(x, h)$ is the same gaussian kernel than for the KDE estimation with a bandwidth empirically set to $h = 5$.

**Table S4 - List of primers used in this study for RT-qPCR** (transcripts). Genes used for normalization of RT-qPCR are in italic.

| | **Chicken** | | **Pigeon** | |
|---|---|---|---|---|
| | **Forward** | **Reverse** | **Forward** | **Reverse** |
| **Ngn2** | GCCACACACGTGTTCACATT | CAATCCCTTTGCTCTTCAGC | GCCACACACGTGTTCACATT | CAATCCCTTTGCTCTTCAGC |
| **Hes5.3** | GACAACCTGCTGACACCAAA | CAGCTTCAGCTGCTCAATGC | AGCTGGAGAAAGCCGACATC | AGCCCTCTCTGAAGTCAAACTG |
| **CHRNB2** | CTACGACGGCAGCATCTTCT | TCGTAGGTCCAGGAACGGAA | CACCATGAAGTTCCGCTCCT | GAATCCTCGGGGTTCTCGTT |
| **NeuroD1** | GTGCCCTGCTACTCCAAGAC | TCTGCACGAATGAGACCAGG | ACTCCAAGACGCAGAAGCTC | CACGAAGGAGACCAGGTCAG |
| **NeuroD4** | CCCACTTCCAAAACGCAGTG | CGTTGAAGATGGCGTTGAGC | GGAGAAGTCCCCAGTGTGTG | TCTTGAAGGTCGGTGGCTTC |
| ***EEF1A*** | CCCGAAGTTCCTGAAATCTG | GAAACGACCCAGAGGAGGAT | ATCGTCGTTCTGGCAAGAAG | ATGTCACGCACAGCAAAACG |
| ***GAPDH (1)*** | ATGATCCCTTCATCGATCTG | ATCCACAGTTTCCCGTTCTC | ATGATCCCTTCATCGATCTG | ATCCACAGTTTCCCGTTCTC |
| ***GAPDH (2)*** | CAAGTGGTGGCCATCAATGATC | ACAAGTTTCCCGTTCTCAGC | TCTCTCTGCCAAAGTCCAAGTG | TTCCCATTCTCGGCCTTGAC |
| ***TBP*** | CTGCGCTTATATTCAGCTCTGG | TGCAGGAAAACCCAGTTTCTG | AGAGAACCACGTACTACTGCAC | TTGCAGGAAAACCCAGCTTC |

ACKNOWLEDGMENTS

We are thankful to Marie Frossard for her help in tissue processing, to Philipp Delaunay and Francois Jardin for the supply of pigeon eggs, and adult pigeons (https://www.pigeonneau-normand.com/) and to Marc Plancherel for the supply of adult quails (https://www.oeuf-de-caille.com/). We wish to thank Nicolás Lendínez Bolaños (Geneva veterinary service) for his help in getting access to chicken brain tissues. Tissue processing and confocal microscopy were performed at the Bioimaging Platform of the Faculty of Sciences (http://bioimaging.unige.ch). We wish to thank Christof Bauer for his advice. RT-qPCR and RNA-Seq experiments were performed at the iGE3 genomics platform of the University of Geneva (http://www.ige3.unige.ch/genomics-platform.php). We thank Frederic Schütz (the Swiss Institute of Bioinformatics) for having made possible the completion of RNA sequencing data analysis. We are grateful to Laurent Vallotton (Natural History Museum of Geneva) for the critical reading of the manuscript and for inspiring discussions.

COMPETING INTERESTS

No competing interests declared.

FUNDING

The Swiss National Science Foundation (grant 31003A-149458 to J.-M.M.), the Gene & Vision.ch Foundation and the state of Geneva support our laboratory.

DATA AVAILABILITY

Data from RNA sequencing will be made available at Gene Expression Omnibus (GEO) as soon as the paper is accepted for publication.

# REFERENCES

Anders, S., Pyl, P.T., and Huber, W. (2015). HTSeq--a Python framework to work with high-throughput sequencing data. Bioinformatics *31*, 166-169.

Andrews, S. (2010). FastQC: A Quality Control Tool for High Throughput Sequence Data (Online).

Appunni, S., Anand, V., Khandelwal, M., Gupta, N., Rubens, M., and Sharma, A. (2019). Small Leucine Rich Proteoglycans (decorin, biglycan and lumican) in cancer. Clin Chim Acta *491*, 1-7.

Bagnoli, P., Porciatti, V., Fontanesi, G., and Sebastiani, L. (1987). Morphological and functional changes in the retinotectal system of the pigeon during the early posthatching period. J Comp Neurol *256*, 400-411.

Bostrom, J.E., Dimitrova, M., Canton, C., Hastad, O., Qvarnstrom, A., and Odeen, A. (2016). Ultra-Rapid Vision in Birds. PLoS One *11*, e0151099.

Bringmann, A. (2019). Structure and function of the bird fovea. Anat Histol Embryol *48*, 177-200.

Bringmann, A., Syrbe, S., Gorner, K., Kacza, J., Francke, M., Wiedemann, P., and Reichenbach, A. (2018). The primate fovea: Structure, function and development. Prog Retin Eye Res *66*, 49-84.

Brodier, L., Rodrigues, T., Matter-Sadzinski, L., and Matter, J.M. (2021). A transient decrease in mitochondrial activity contributes to establish the ganglion cell fate in retina adapted for high acuity vision. Dev Biol *469*, 96-110.

Charvet, C.J., and Striedter, G.F. (2011). Developmental Modes and Developmental Mechanisms can Channel Brain Evolution. Front Neuroanat *5*, 4.

Cherix, A., Brodier, L., Poitry-Yamate, C., Matter, J.M., and Gruetter, R. (2020). The Appearance of the Warburg Effect in the Developing Avian Eye Characterized In Ovo: How Neurogenesis Can Remodel Neuroenergetics. Invest Ophthalmol Vis Sci *61*, 3.

Chiodini, F., Matter-Sadzinski, L., Rodrigues, T., Skowronska-Krawczyk, D., Brodier, L., Schaad, O., Bauer, C., Ballivet, M., and Matter, J.M. (2013). A positive feedback loop between ATOH7 and a Notch effector regulates cell-cycle progression and neurogenesis in the retina. Cell Rep *3*, 796-807.

Clarke, P.G., and Whitteridge, D. (1976). The projection of the retina, including the 'red area' on to the optic tectum of the pigeon. Q J Exp Physiol Cogn Med Sci *61*, 351-358.

Collins, C.E., Airey, D.C., Young, N.A., Leitch, D.B., and Kaas, J.H. (2010). Neuron densities vary across and within cortical areas in primates. Proc Natl Acad Sci U S A *107*, 15927-15932.

Cowey, A., and Rolls, E.T. (1974). Human cortical magnification factor and its relation to visual acuity. Exp Brain Res *21*, 447-454.

Daniel, P.M., and Whitteridge, D. (1961). The representation of the visual field on the cerebral cortex in monkeys. J Physiol *159*, 203-221.

Davis, M.P.A., van Dongen, S., Abreu-Goodger, C., Bartonicek, N., and Enright, A.J. (2013). Kraken: A set of tools for quality control and analysis of high-throughput sequence dat. Methods *63*, 41-49.

Deckx, S., Heymans, S., and Papageorgiou, A.P. (2016). The diverse functions of osteoglycin: a deceitful dwarf, or a master regulator of disease? FASEB J *30*, 2651-2661.

Dobin, A., Davis, C.A., Schlesinger, F., Drenkow, J., Zaleski, C., Jha, S., Batut, P., Chaisson, M., and Gingeras, T.R. (2013). STAR: ultrafast universal RNA-seq aligner. Bioinformatics *29*, 15-21.

Evsyukova, I., Plestant, C., and Anton, E.S. (2013). Integrative mechanisms of oriented neuronal migration in the developing brain. Annu Rev Cell Dev Biol *29*, 299-353.

Feng, Y., and Walsh, C.A. (2004). Mitotic spindle regulation by Nde1 controls cerebral cortical size. Neuron *44*, 279-293.

Galileo, D.S., Majors, J., Horwitz, A.F., and Sanes, J.R. (1992). Retrovirally introduced antisense integrin RNA inhibits neuroblast migration in vivo. Neuron *9*, 1117-1131.

Gray, G.E., and Sanes, J.R. (1991). Migratory paths and phenotypic choices of clonally related cells in the avian optic tectum. Neuron *6*, 211-225.

Gruber, R., Zhou, Z., Sukchev, M., Joerss, T., Frappart, P.O., and Wang, Z.Q. (2011). MCPH1 regulates the neuroprogenitor division mode by coupling the centrosomal cycle with mitotic entry through the Chk1-Cdc25 pathway. Nat Cell Biol *13*, 1325-1334.

Hagen, S.J. (2017). Non-canonical functions of claudin proteins: Beyond the regulation of cell-cell adhesions. Tissue Barriers *5*, e1327839.

Hamdi, F.A., and Whitteridge, D. (1954). The representation of the retina on the optic tectum of the pigeon. Q J Exp Physiol Cogn Med Sci *39*, 111-119.

Ho, C.L.A., Zimmermann, R., Florez Weidinger, J.D., Prsa, M., Schottdorf, M., Merlin, S., Okamoto, T., Ikezoe, K., Pifferi, F., Aujard, F*., et al.* (2021). Orientation Preference Maps in Microcebus murinus Reveal Size-Invariant Design Principles in Primate Visual Cortex. Curr Biol *31*, 733-741 e737.

Jarvis, E.D., Mirarab, S., Aberer, A.J., Li, B., Houde, P., Li, C., Ho, S.Y., Faircloth, B.C., Nabholz, B., Howard, J.T*., et al.* (2014). Whole-genome analyses resolve early branches in the tree of life of modern birds. Science *346*, 1320-1331.

Karamanou, K., Franchi, M., Proult, I., Rivet, R., Vynios, D., and Brezillon, S. (2021). Lumican Inhibits In Vivo Melanoma Metastasis by Altering Matrix-Effectors and Invadopodia Markers. Cells *10*.

King, W.M. (1990). Nicotinic depolarization of optic nerve terminals augments synaptic transmission. Brain Res *527*, 150-154.

Knudsen, E.I. (2011). Control from below: the role of a midbrain network in spatial attention. Eur J Neurosci *33*, 1961-1972.

Lang, P.Y., Nanjangud, G.J., Sokolsky-Papkov, M., Shaw, C., Hwang, D., Parker, J.S., Kabanov, A.V., and Gershon, T.R. (2016). ATR maintains chromosomal integrity during postnatal cerebellar neurogenesis and is required for medulloblastoma formation. Development *143*, 4038-4052.

LaVail, J.H., and Cowan, W.M. (1971a). The development of the chick optic tectum. I. Normal morphology and cytoarchitectonic development. Brain Res *28*, 391-419.

LaVail, J.H., and Cowan, W.M. (1971b). The development of the chick optic tectum. II. Autoradiographic studies. Brain Res *28*, 421-441.

Lee, Y., Shull, E.R., Frappart, P.O., Katyal, S., Enriquez-Rios, V., Zhao, J., Russell, H.R., Brown, E.J., and McKinnon, P.J. (2012). ATR maintains select progenitors during nervous system development. EMBO J *31*, 1177-1189.

Love, M.I., Huber, W., and Anders, S. (2014). Moderated estimation of fold change and dispersion for RNA-seq data with DESeq2. Genome Biol *15*, 550.

Malpeli, J.G., and Baker, F.H. (1975). The representation of the visual field in the lateral geniculate nucleus of Macaca mulatta. J Comp Neurol *161*, 569-594.

Manns, M., and Gunturkun, O. (1997). Development of the retinotectal system in the pigeon: a cytoarchitectonic and tracing study with cholera toxin. Anat Embryol (Berl) *195*, 539-555.

Martin, M. (2011). Cutadapt removes adapter sequences from high-throughput sequencing reads. 2011 *17*, 3.

Matter-Sadzinski, L., Matter, J.M., Ong, M.T., Hernandez, J., and Ballivet, M. (2001). Specification of neurotransmitter receptor identity in developing retina: the chick ATH5 promoter integrates the positive and negative effects of several bHLH proteins. Development *128*, 217-231.

Matter, J.M., Matter-Sadzinski, L., and Ballivet, M. (1990). Expression of neuronal nicotinic acetylcholine receptor genes in the developing chick visual system. EMBO J *9*, 1021-1026.

Nobrega-Pereira, S., Kessaris, N., Du, T., Kimura, S., Anderson, S.A., and Marin, O. (2008). Postmitotic Nkx2-1 controls the migration of telencephalic interneurons by direct repression of guidance receptors. Neuron *59*, 733-745.

Provis, J.M., Dubis, A.M., Maddess, T., and Carroll, J. (2013). Adaptation of the central retina for high acuity vision: cones, the fovea and the avascular zone. Prog Retin Eye Res *35*, 63-81.

Prum, R.O., Berv, J.S., Dornburg, A., Field, D.J., Townsend, J.P., Lemmon, E.M., and Lemmon, A.R. (2015). A comprehensive phylogeny of birds (Aves) using targeted next-generation DNA sequencing. Nature *526*, 569-573.

Ramón y Cajal, S. (1893). La Rétine des Vertébrés. La Cellule *9*, 119-257.

Rockel, A.J., Hiorns, R.W., and Powell, T.P. (1980). The basic uniformity in structure of the neocortex. Brain *103*, 221-244.

Rodrigues, T., Krawczyk, M., Skowronska-Krawczyk, D., Matter-Sadzinski, L., and Matter, J.M. (2016). Delayed neurogenesis with respect to eye growth shapes the pigeon retina for high visual acuity. Development *143*, 4701-4712.

Rolls, E.T., and Cowey, A. (1970). Topography of the retina and striate cortex and its relationship to visual acuity in rhesus monkeys and squirrel monkeys. Exp Brain Res *10*, 298-310.

Rosa, M.G., Fritsches, K.A., and Elston, G.N. (1997). The second visual area in the marmoset monkey: visuotopic organisation, magnification factors, architectonical boundaries, and modularity. J Comp Neurol *387*, 547-567.

Roztocil, T., Matter-Sadzinski, L., Alliod, C., Ballivet, M., and Matter, J.M. (1997). NeuroM, a neural helix-loop-helix transcription factor, defines a new transition stage in neurogenesis. Development *124*, 3263-3272.

Schwab, I.R., Dubielzig, R.R., and Schobert, C. (2012). Evolution's Witness: How Eyes Evolved (OUP USA).

Sergaki, M.C., and Ibanez, C.F. (2017). GFRalpha1 Regulates Purkinje Cell Migration by Counteracting NCAM Function. Cell Rep *18*, 367-379.

Shibata, E., Kiran, M., Shibata, Y., Singh, S., Kiran, S., and Dutta, A. (2016). Two subunits of human ORC are dispensable for DNA replication and proliferation. Elife *5*.

Sinha, R., Hoon, M., Baudin, J., Okawa, H., Wong, R.O.L., and Rieke, F. (2017). Cellular and Circuit Mechanisms Shaping the Perceptual Properties of the Primate Fovea. Cell *168*, 413-426 e412.

Slonaker, J.R. (1897). A comparative study of the area of acute vision in vertebrates. Journal of Morphology *13*, 445-502.

Srinivasan, S., Carlo, C.N., and Stevens, C.F. (2015). Predicting visual acuity from the structure of visual cortex. Proc Natl Acad Sci U S A *112*, 7815-7820.

Titmus, M.J., Tsai, H.J., Lima, R., and Udin, S.B. (1999). Effects of choline and other nicotinic agonists on the tectum of juvenile and adult Xenopus frogs: a patch-clamp study. Neuroscience *91*, 753-769.

Vandesompele, J., De Preter, K., Pattyn, F., Poppe, B., Van Roy, N., De Paepe, A., and Speleman, F. (2002). Accurate normalization of real-time quantitative RT-PCR data by geometric averaging of multiple internal control genes. Genome Biol *3*, RESEARCH0034.

Wang, L., Wang, S., and Li, W. (2012). RSeQC: quality control of RNA-seq experiments. Bioinformatics *28*, 2184-2185.

Yang, J., Fan, L., Liao, X., Cui, G., and Hu, H. (2021). CRTAC1 (Cartilage acidic protein 1) inhibits cell proliferation, migration, invasion and epithelial-mesenchymal transition (EMT) process in bladder cancer by downregulating Yin Yang 1 (YY1) to inactivate the TGF-beta pathway. Bioengineered *12*, 9377-9389.